N-1,2,3-Triazole-Isatin Derivatives for Cholinesterase and β-Amyloid Aggregation Inhibition: *A Comprehensive Bioassay Study*

Carolina S. Marques,[a] Óscar López,[b] Donatella Bagetta,[c,d] Elisabete P. Carreiro,[a] Sabrina Petralla[e], Manuela Bartolini[e], Matthias Hoffmann[f], Stefano Alcaro[c,d], Barbara Monti[e], Maria Laura Bolognesi[e], Michael Decker[f], José G. Fernández-Bolaños[b] and Anthony J. Burke,[a,g*]

[a]Centro de Química de Évora, University of Évora, Institute for Research and Advanced Studies, Rua Romão Ramalho, 59, 7000 Évora, Portugal
[b]Departamento de Química Orgánica, Facultad de Química, Universidad de Sevilla, Apartado 1203, E-41071, Seville, Spain
[c]Net4Science Academic Spin-Off, University "Magna Græcia" of Catanzaro, Campus Universitario "S.Venuta", Catanzaro, Italy
[d]Department of "Scienze della Salute", University "Magna Græcia" of Catanzaro, Campus Universitario "S. Venuta", Catanzaro, Italy
[e]Department of Pharmacy and Biotechnology, Alma Mater Studiorum, University of Bologna, via Belmeloro 6/via Selmi 3, 40126 Bologna, Italy.
[f]Pharmaceutical and Medicinal Chemistry, Institute of Pharmacy and Food Chemistry, Julius Maximilian University Würzburg, Am Hubland, D-97074 Würzburg, Germany.
[g]Chemistry Department, School of Science and Technology, University of Évora, Rua Romão Ramalho 59, 7000-671 Évora, Portugal.

*Corresponding author: Centro de Química de Évora and Chemistry Department, School of Science and Technology, University of Évora, Rua Romão Ramalho 59, 7000-671 Évora, Portugal
Email address: ajb@uevora.pt (A. J. Burke)

Abstract

Our goal was the evaluation of a series of *N*-1,2,3-triazole-isatin derivatives for multi-target activity which included cholinesterase (ChE) inhibition and β-amyloid (Aβ) peptide anti-aggregation. The compounds have shown considerable promise as butyrylcholinesterase (BuChE) inhibitors. Although the inhibition of eel acetylcholinesterase (*ee*AChE) was weak, the inhibitions against *equine* BuChE (*eq*BuChE) and *human* BuChE (*h*BuChE) were more significant with a best inhibition against *eq*BuChE of 0.46 μM. In some cases, these molecules gave better inhibitions for *h*BuChE than *eq*BuChE. For greater insights into their mode of action, molecular docking studies were carried out subsequent STD-NMR validation. In addition, some of these compounds showed weak Aβ anti-aggregation activity.

Hepatotoxicity studies showed that they were non-hepatoxic and neurotoxicity studies using neurite outgrowth experiments led to the conclusion that these compounds are only weakly neurotoxic.

Keywords

Isatin; oxindole; 1,2,3-triazole; butyrylcholinesterase; β-amyloid inhibition; hepatotoxicity; neurotoxicity.

1. Introduction

Presently the development of new drugs to combat Alzheimer's disease (AD) is a very critical issue for all stake-holders, especially considering the huge number of sufferers world-wide and the numbers that are forecasted for the next 20-30 years [1-3]. Neurodegenerative diseases such as AD are a topic of major concern due to increased life expectancy leading to an ever-increasing ageing world population. AD is associated with neuronal malfunction due to the build-up of β-amyloid (Aβ) plaques outside the neuron leading to neuronal death by disrupting the cell-to-cell communication process, as well as the formation of abnormal tau proteins inside neurons leading to blockage of nutrient transport into the neurons [4]. Moreover, AD is characterized by decreased levels of the neurotransmitter acetylcholine (ACh), vital in maintaining normal cognitive function (cholinergic hypothesis)[5]. As a result, inhibition of acetylcholinesterase (AChE) and butyrylcholinesterase (BuChE) - the enzymes devoted to the breakdown of ACh in the brain - is the standard approach for maintaining the levels of ACh. Currently, there are only three FDA approved drugs on the market which act as cholinesterase inhibitors. These include rivastigmine, galantamine and donepezil (Figure 1). Although AChE and BuChE share about 65% structural homology, the main difference occurs in the so-called acyl binding pocket (which interacts with the ACh acyl group) and the Peripheral Anionic Site (PAS, which is thought to be involved in Aβ binding) [6]. In fact, in AChE, the acyl binding site contains both Phe295 and Phe297 which restrict the size of the gorge, whilst BuChE contains two aliphatic residues, Leu286 and Val288. Furthermore, 6 out of 14 aromatic residues lining the AChE gorge rim and the so-called PAS (see below) are replaced by aliphatic residues in BuChE [7]. As a result, the BuChE gorge is about 200 $Å^3$ larger than the AChE gorge [6c].

In 1993 Wright *et al.* demonstrated that AChE has other non-catalytic functions and colocalizes with Aβ in neuritic plaques [8]. AChE can act as a molecular chaperon and accelerate the formation of Aβ–fibrils, forming stable complexes. It has been suggested that the aggregation-promoting action of AChE is mediated by the PAS [9-11], which includes an aromatic triad that consists of Tyr72, Tyr124 and Trp286 [10]. Studies have shown that occupancy of the PAS by an appropriate phenanthridine inhibitor **I** (Figure 2) could block the entry to the AChE active site [11]. The polyamine-tacrine analogue **II** was developed to simultaneously block both the PAS and the catalytic active site (CAS), thus retarding AChE ability to promote the formation of Aβ–fibrils and ACh hydrolysis [11]. BuChE is believed to play a minor role in regulating brain ACh levels in a healthy brain, but, becomes more evident in the brain of patients with advanced forms of AD having been detected in both Aβ plaques and neurofibrillary tangles [12]. Diamant *et al.* showed that both BuChE and a synthetic peptide derived from the BuChE C terminus associate with soluble Aβ conformers with the result that the onset of Aβ fibril formation is delayed with a decrease in the rate of formation of the Aβ fibrils [13]. Transgenic mice that over-expressed human mutant Amyloid Precursor Protein (APP) that were administered the BuChE-selective inhibitor cymserine and analogues showed lower levels of Aβ peptide compared to the controls [14]. Guillozer *et al*. suggested BuChE becomes associated with Aβ plaques at approximately the same time that the Aβ deposits assume a compact β-pleated conformation commonly observed at the advanced stages of the disease [15]. It was shown that apolipoprotein E4 (APOE) facilitates formation of molecular complexes between BuChE and Aβ [16a]. They also provided evidence that the amyloid peptides formed stable complexes with human BuChE (*h*BuChE) and suggested from key molecular modelling studies on BuChE and two isoforms of Aβ, namely $Aβ_{40}$ and $Aβ_{42}$,

the 40- and 42 amino acid long peptides respectively, that this interaction causes a widening of the mouth of the gorge and/or a more hydrophobic environment for entrance of the substrate (Try288 was identified as an important element in the interaction of these peptides with the so-called PAS of BuChE, which is presumed to be via hydrophobic interactions). A recent study has shown that BuChE inhibition bestows very important neuroprotective effects [16b]. After inducing AD-like cognitive dysfunction in mice, via intracerebroventricular administration of oligomerized $A\beta_{25-35}$ peptide, it was found that some serious neuroprotective effects were observed when certain carbamic BuChE inhibitors were administered [16b].

Oxindoles are a group of privileged frameworks that show a diverse range of pharmacological activities, including, anti-cancer, anti-HIV, antidiabetic, antibacterial, antioxidant activities, kinase inhibition [17-19] and are an important component of some ChE inhibitors (Figure 1) [20-22]. Our group developed a selective *eq*BuChE inhibitor (Figure 1) containing an oxindole core which afforded good levels of inhibition (IC_{50} = 6.61 μM) [23a,b]. Furthermore, isatin (2,3-dioxoindole) demonstrates Aβ anti-aggregation activity and it was shown to significantly prevent binding of specific Aβ binding proteins to Aβ [24]. A series of arylhydrazono-1*H*-2-indolinones which exhibited Aβ anti-aggregating properties (specifically, towards $A\beta_{40}$ aggregation) with IC_{50} values in the low micromolar range have also been devised (Figure 3) [25]. Rhynchophylline (RIN) [26a] (also known as an NMDA receptor antagonist) and Isorhynchophylline (ISRIN) [26b](Figure 3) were found to supress the soluble $A\beta_{42}$ oligomers-induced enhancement of spontaneous discharge in a concentration-dependent manner, thus counteracting the deleterious effect of $A\beta_{42}$ on the neural circuit (RIN) or acting as a protective agent (ISRIN) against $A\beta_{25-35}$ induced neurotoxicity in PC12 cells.

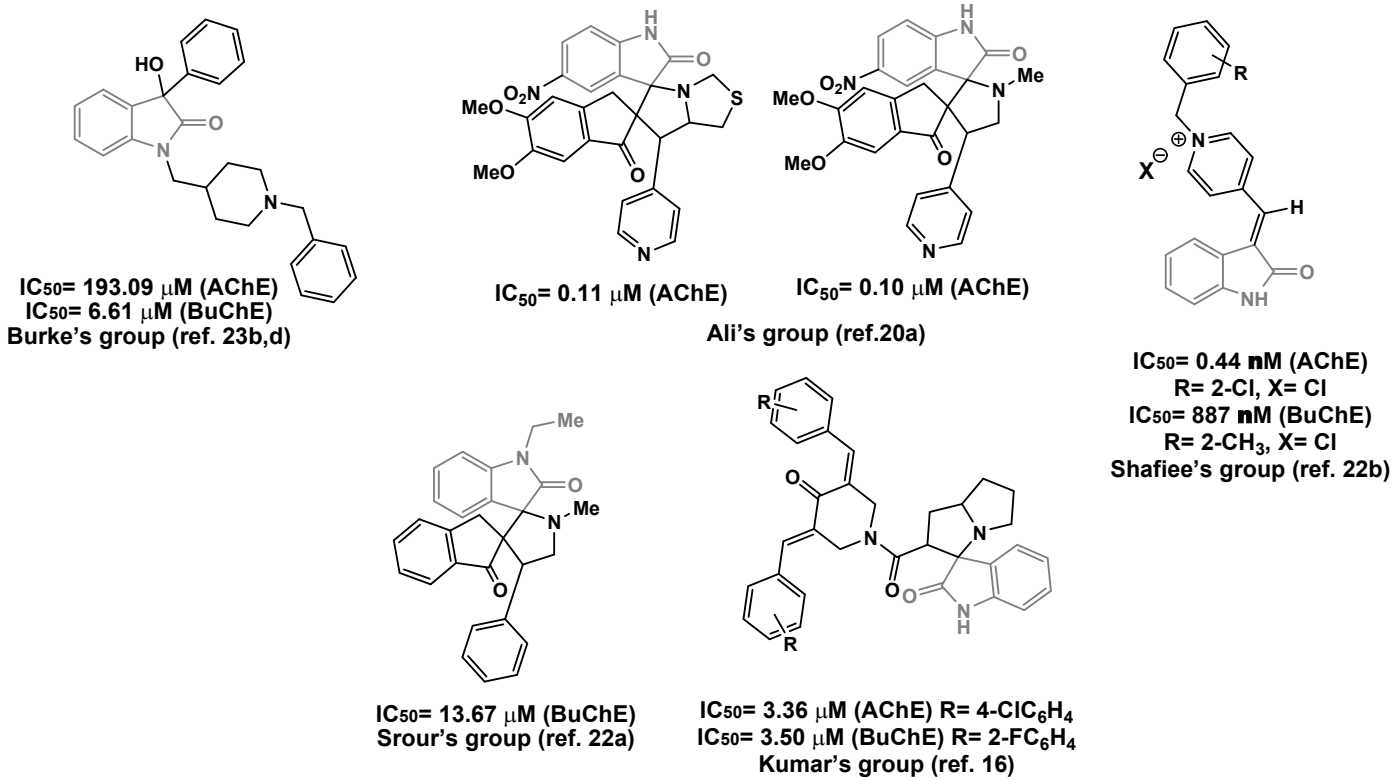

Figure 1. FDA approved ChE inhibitors (in the upper left side box) and lead ChE inhibitor compounds (in most cases the origin of the ChE is indicated).

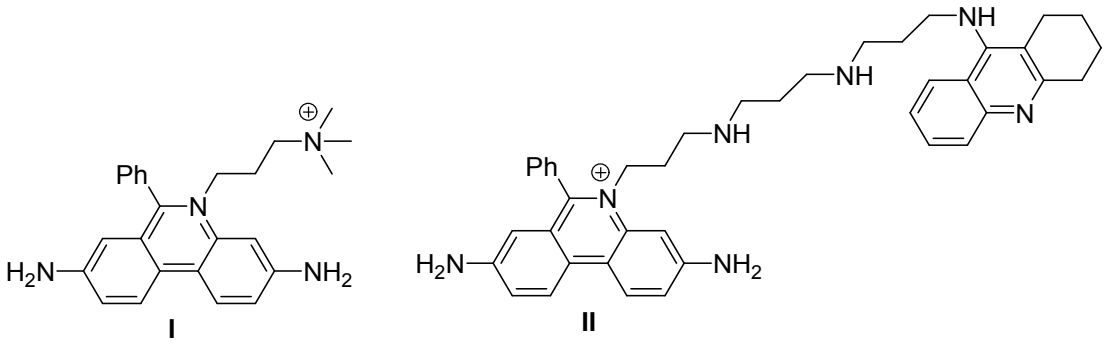

Figure 2. Propidium based AChE inhibitors with Aβ anti-aggregation activity (*hr* = human recombinant).

The 1,2,3-triazole unit has been associated with potent biological activities (Figure 4, (a)) [27, 28]. It is present in compounds that exhibit ChE inhibition – although it seems that its role is less important for binding with the key enzymatic sites than the other moieties. Compound **III** is a good and selective AChE inhibitor [29] and the tacrine hybrid **IV** was shown to be a non-selective inhibitor of both AChE and BuChE [28]. Novel sarsasapogenin-triazole hybrids (e.g. compound **V)** were developed for potent $A\beta_{1\text{-}42}$ aggregation inhibition [31]. Notably, an extremely potent triazole-linked bivalent AChE inhibitor was obtained through a *in situ* click-chemistry approach

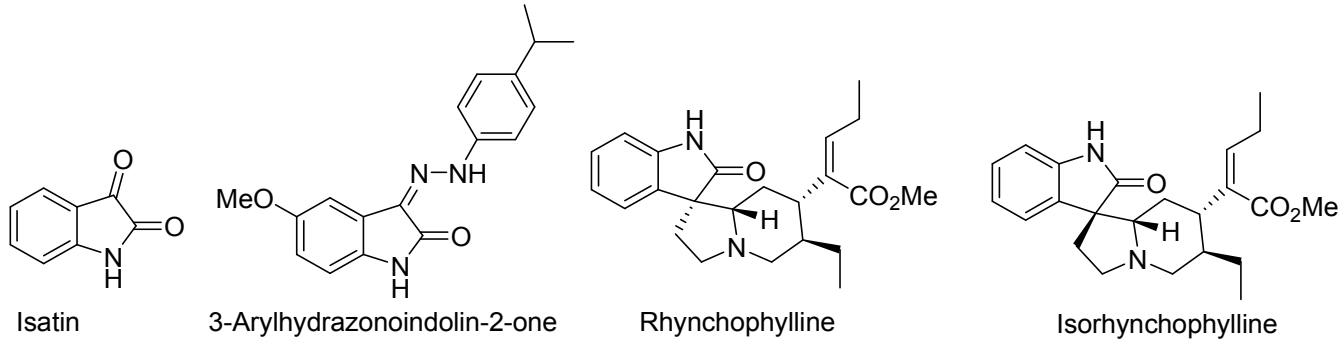

Figure 3. Some isatin-based Aβ aggregation inhibitors.

Oxindole-1,2,3-triazole hybrids are known to display significant biological activities [32-35]. We have synthesized a family of novel oxindole-1,2,3-triazole hybrids which exhibited lymphoma anti-proliferation effects [36]. In the context of the aforementioned discussion we deduced, based on previous studies, that such compounds would have the capacity to straddle and fill the active site gorge of both AChE and BuChE and have potential to bind with the PAS and some of the other key binding regions (acyl binding pocket and/or the CAS) in the ChE active site (this hypothesis was supported by key molecular docking studies discussed below). It should also be noted that numerous studies have shown the importance of the triazole unit in positioning the ligand in the enzyme binding site (via appropriate non-covalent interactions).

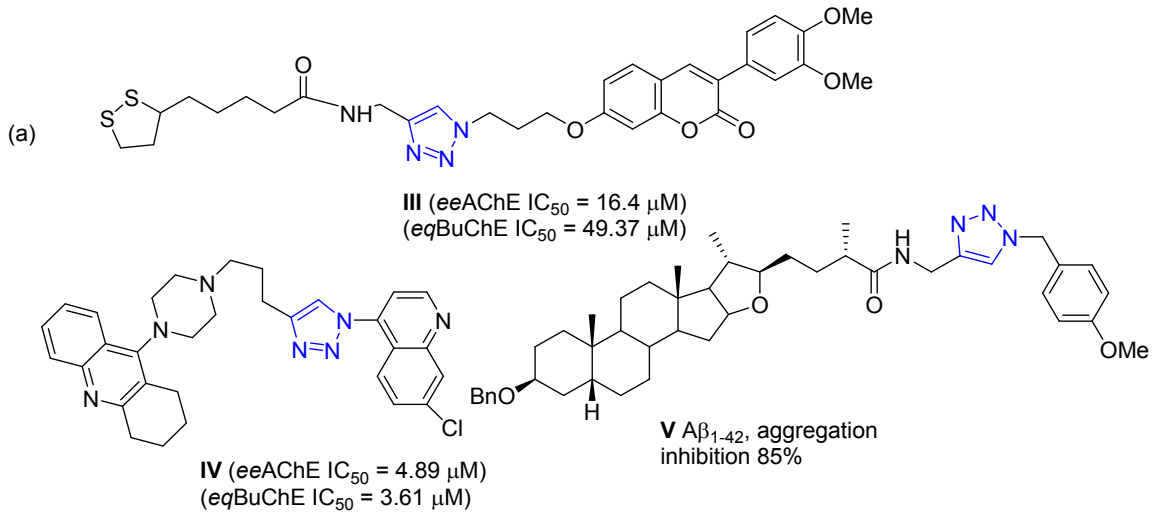

Figure 4. 1,2,3-Triazole containing ChE inhibitors and Aβ aggregation inhibitors.

In this study we report our results on screening a number of isatin-1,2,3-triazole molecules for *ee*AChE and BuChE inhibition, for anti-aggregation activity toward Aβ, in addition to some cell-based assays to determine the hepatotoxicity and neurotoxicity of these compounds.

2. Results and Discussion

2.1. Chemistry

Our goal was to test both isatin-triazoles **(1)** and 3-aryl-2-hydroxyoxindole-triazoles **(2)** (Scheme 1). The synthesis of *N*-1,2,3-triazole-isatin derivatives **(1a-c)** and the *N*-(1,2,3-triazolmethyl)-3-hydroxy-3-aryloxindole derivatives **(2a-i)** (Scheme 1) was previously reported [36]. In addition, and for comparative purposes, we prepared the corresponding (*S*)-3-hydroxy-1-((1-(((1*S*,2*S*,5*R*)-5-isopropyl-2-methylcyclohexyl)-1*H*-1,2,3-triazol-4-yl)methyl)-3-phenylindolin-2-one **(2j)** using a standard metal catalysed arylation procedure with compound **(1b)** as substrate. The desired compound **(2j)** was obtained in 63% yield using (*R*)-BINAP as chiral ligand (Scheme 2) (since we obtained a single diastereoisomer and based on literature precedent [23b] the following stereochemical configuration was assigned (Scheme 2)). The compounds showed a purity of >98% by NMR spectroscopy.

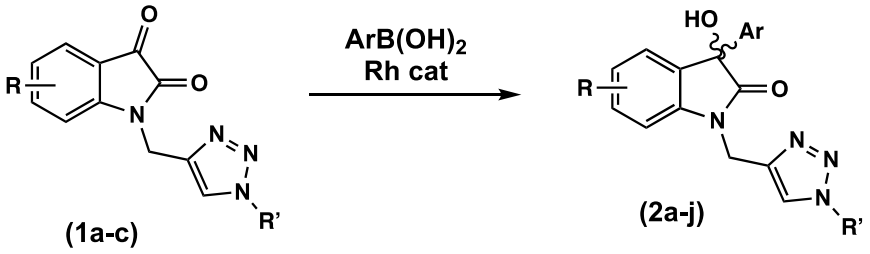

Compound	R	R'	Ar
1a	H	Bn	-
1b	H	(1*S*,2*S*,5*R*)-neomenthyl	-
1c	5-Me	Bn	-
2a	H	Bn	C_6H_5 (*S*)
2b	H	Bn	2-naphthyl (*R*)
2c	H	Bn	4-MeC_6H_4 (*R*)
2d	H	Bn	4-FC_6H_4 (*S*)
2e	H	Bn	4-MeOC_6H_4 (*R*)
2f	H	Bn	3-thienyl (*S*)
2g	H	Bn	3-thienyl (*R*)
2h	H	Bn	3-HOC_6H_4 (*S*)

2i	H	Butyl	C_6H_5 (*S*)
2j	H	(1*S*,2*S*,5*R*)-neomenthyl	C_6H_5 (*S*)

Scheme 1. Chemically modified oxindole derivatives **(2).**

Spiro-oxindoles have emerged as privileged scaffolds for medicinal chemistry [19]. Ketal-type spiro-oxindoles have recently been reported by Silva's group and evaluated for their hypnotic, anxiolytic and antinociceptive activities [37] and by Wood's group who showed positive allosteric modulation of the human muscarinic M1 receptor with their ketal-type spiro-oxindoles [38]. With this in mind, we introduced a dioxolane group into our family affording the spiro-ketal-oxindole **(2k)** (obtained in 79% yield) (Scheme 2). Besides, the protection of the 3-carbonyl group as an acetal group was important to gain insight into the role of the isatin-3-carbonyl group of our inhibitors during enzymatic inhibition (see below).

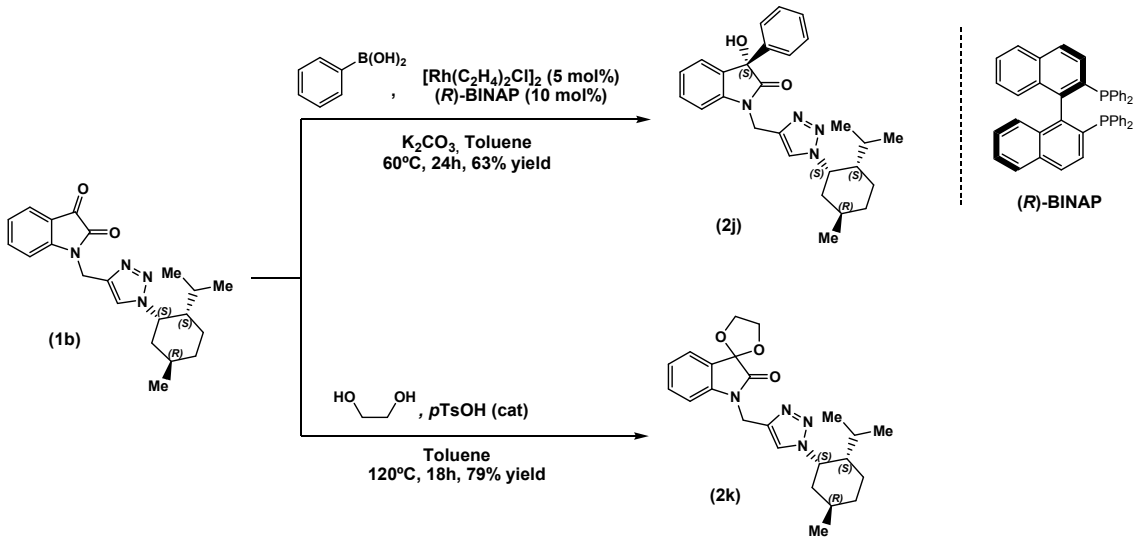

Scheme 2. The synthesis of *N*-(1,2,3-triazolmeyhyl)-oxindole derivatives **(2j)** and **(2k)**.

2.2. Pharmacological evaluation

2.2.1. Cholinesterase inhibitory activity, SAR and kinetic studies

Initially the inhibitory activity of the compounds **(1)** and **(2)** was screened *in vitro* on *ee*AChE and *eq*BuChE at an initial concentration of 100 μM; such enzymes are considered as good models due to their structural similarity with the human isoform. The preliminary results are listed in Table s1 (supporting information).

In general, the tested compounds displayed poor inhibition of *ee*AChE (see Table 1). These compounds were selective for BuChE over AChE (see Table 1). In particular, compounds **(1b)**, **(1c)**, **(2a)**, **(2c-f), (2j)** and **(2k)** gave much lower IC_{50} values (Table 1). Compound **(1b)** presented a remarkable IC_{50} value for *eq*BuChE of 0.46μM (Table 1, entry 2), and shows an excellent selectivity index of >217 towards BuChE, which is the most prevalent cholinesterase for those with advanced stages of Alzheimer's disease. We were intrigued to test our compounds *in vitro* in *h*BuChE. Considering the weak values achieved in the *ee*AChE model and the high associated cost of *h*AChE, this study was limited only to *h*BuChE.

Table 1. IC_{50} values for *eq*BuChE and *h*BuChE with *N*-1,2,3-triazole-isatin derivatives **(1)** and **(2)**.

Entry	Compound[a]	*ee*AChE **IC_{50} (μM)[b]**	*eq*BuChE **IC_{50} (μM)[b,c]** ($pIC_{50} \pm$ SEM)	*h*BuChE **IC_{50} (μM)[c]** ($pIC_{50} \pm$ SEM)
1	**1a**	>100	14.00 (4.86 ± 0.22)	2.20 (5.65 ± 0.03)
2	**1b**	>100	0.46 (6.35 ± 0.13)	0.51 (6.29 ± 0.02)
3	**1c**	>100	15.70 (4.81 ± 0.31)	21.50 (4.67 ± 0.03)
4	**2a**	>100	41.00 (4.40 ± 0.85)	10.00 (5.00 ± 0.03)
5	**2b**	>100	Not soluble	> 100 Not soluble
6	**2c**	>100	52.60 (4.31 ± 0.22)	15.90 (4.80 ± 0.04)
7	**2d**	>100	77.90 (4.11 ± 0.36)	>100
8	**2e**	>100	>100	>100
9	**2f**	>100	72.30 (4.14 ± 0.36)	>100
10	**2g**	>100	>100	> 100
11	**2h**		>100	>100
12	**2i**	>100	>100	>100
13	**2j**	>100	2.20 (5.67 ± 0.09)	4.20 (5.38 ± 0.03)
14	**2k**	90 (4.05 ± 0.54)	3.60 (5.45 ± 0.36)	25.20 (4.60 ± 0.02)
15	**Galantamine**	2.7 ± 0.20 (5.58± 0.03)	10.00 (4.99 ± 0.36)	

[a]See structures in Schemes 1 and 2.
[b]Average of 4-5 different inhibitor concentrations and data obtained in duplicate.
[c] At 0.452 μM substrate concentration.

In the case of compound **(1b)** it was found to be slightly less active against *h*BuChE, with a value of 510 nM. In the case of *h*BuChE, **(1a)** gave an IC_{50} value of 2.2 μM which was better than that obtained for *ee*BuChE (14 μM). In the case of both **(2a)** and **(2c)** these compounds registered better inhibitions with *h*BuChE than with *eq*BuChE, but in the case of compounds **(2d)**-**(2f)** and **(2k)** it was the opposite.

In the case of the most potent inhibitors, i.e. compounds **(1a-c)**, **(2a)**, **(2c)** and **(2j-k)** Ellman's assay was conducted in order to calculate the inhibition constant (K_i) (see Supporting Information for more details, Fig. s8-s16). Graphical analysis of the Cornish-Bowden plots for the *eq*BuChE activity afforded both K_{ia} and K_{ib} values (Table 2, and also see supporting information for the graphs). These kinetic studies confirm differences in the mode of inhibition, for the screened inhibitors; for instance **(1a)** and **(2k)** were shown to demonstrate competitive inhibition, **(1c)**, **(2a)** and **(2j)** non-competitive and **(1b)** and **(2c)** mixed inhibitors. From analysis of this data, it was very

difficult to observe any specific trends between structure and the type of observed inhibition (for instance all compounds **(1a)** to **(1c)** having an analogous structural core, showed disparate modes of inhibition).

Table 2. Kinetic parameters for *eq*BuChE inhibition by some selected compounds.[a]

Entry	Compound	K_{ia}/μM	K_{ib}/μM	Mode of inhibition
1	**1a**	16.00 ± 2.00	---	Competitive
2	**1b**	0.16 ± 0.04	0.090 ± 0.030	Mixed
3	**1c**	14.00 ± 2.00	14.00 ± 2.00	Non-competitive
4	**2a**	21.00 ± 2.00	21.00 ± 2.00	
5	**2c**	34.00 ± 3.00	10.00 ± 3.00	Mixed
6	**2j**	1.80 ± 0.20	1.80 ± 0.20	Non-competitive
7	**2k**	21.00 ± 20	---	Competitive
8	**Galantamine**	6.20 ± 0.40	---	

[a] Inhibition constants were obtained using 3-6 inhibitor concentrations, and data are expressed as the mean ± SD of two independent measurements. K_{ia} refers to the inhibition constant for the inhibitor binding the free enzyme. K_{ib} refers to the inhibition constant for the inhibitor binding the ES complex

2.2.2. Aβ aggregation studies

Based on the discussion given previously, and particularly on the work of Medvedev *et al.* [24] we studied the effect of our oxindole containing molecules on $A\beta_{1-42}$ self-aggregation. While the 40-residue peptide $A\beta_{1-40}$ is the most abundant Aβ isoform in the brain, the 42-amino-acid long $A\beta_{1-42}$ is the most amyloidogenic and most prone to aggregate into neurotoxic aggregates. Thus, compounds (**1a**)-(**1c**), **(2j)** and **(2k)** were assayed at a 1:1 ratio using a thioflavin T (ThT)-based fluorescence assay. Experiments were carried out at 30°C in order to get a suitable aggregation profile (suitable lag and exponential phases) within 24h, following a previously optimized and validated protocol [42]. Proper blanks were acquired in order to exclude optical interference by the tested compounds at the excitation and emission wavelengths (see Experimental section).
Inhibition percentages listed in Table 3 imply that these hybrids prevent amyloid self-aggregation only at a very limited extent, in all cases at <20%.
To note, compounds **(1a)** and **(1c)** showing a slightly higher activity are characterized by an isatin unit. The fact that **(2k)** (with the protected 3-carbonyl group) gave the lowest activity was a strong indication of the role of the 3-carbonyl group of isatin in this process.

Table 3. Inhibition of $A\beta_{42}$ self-aggregation using the thioflavin-T fluorescence (ThT) assay (see section 4.3)

Entry	Compound	% inhibition $A\beta_{42}$ self-aggregation ± SEM/SD [a]
1	**1a**	16.80 ± 2.50
2	**1b**	11.50 ± 4.20
3	**1c**	14.80 ± 3.40

4	**2j**	13.30 ± 5.00
5	**2k**	8.30 ± 2.80
6	**Curcumin**	80.40 ± 5.30

[a]Inhibition of $A\beta_{42}$ self-aggregation investigated by the thioflavin-T fluorescence assay. Assays were carried out in the presence of 50 μM inhibitor and 50 μM $A\beta_{42}$ ([I]=[$A\beta_{42}$]); Data are the mean of two independent experiments each performed in duplicate. n.a. = % inhibition lower than 5 %.

Furthermore, in the case of the observed activities it is not known if this anti-aggregation is due to ChE induced inhibition (blockage at the ChE-Aβ binding site) or via direct interaction with the Aβ peptides inhibiting the self-aggregation process, albeit there are strong indications of the later mechanism in the case of the isatin containing compounds. Never-the-less, due to the low levels of aggregation inhibition observed the mode of inhibition was of lower importance.

2.2.3. Docking studies for accessing Cholinesterase inhibitory activity

The bioassay studies discussed above show that our oxindole/isatin-triazole molecules are selective for BuChE inhibition. To gain further insights into the nature of the interactions between our oxindole/isatin-triazole molecules and BuChE we conducted a programmed set of docking experiments. These molecular modelling studies were carried out by docking some of our selected inhibitors into the BuChE active site (Figure 5).

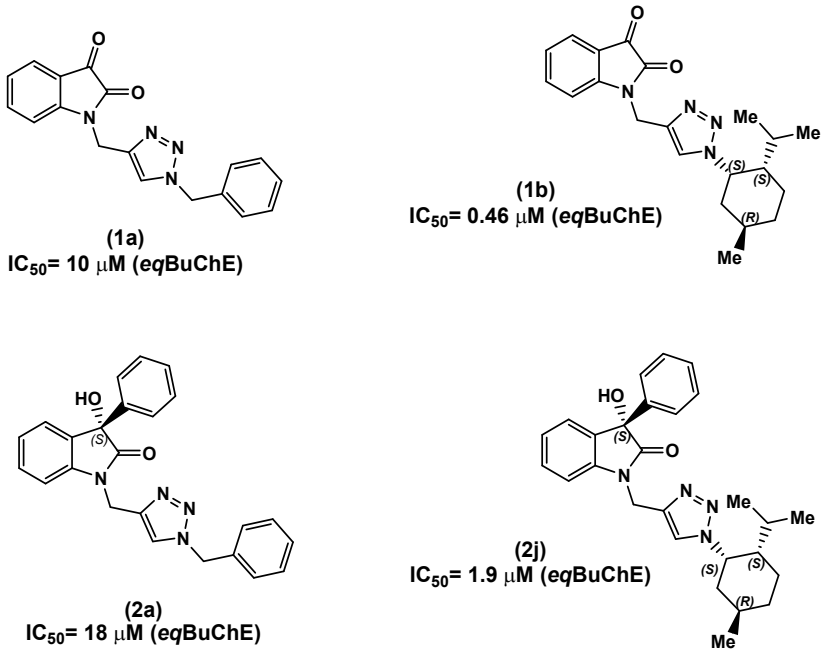

Figure 5. The oxindole/isatin-triazoles subjected to docking studies with *h*BuChE.

The aforementioned docking simulations were performed using the refined X-ray crystal structure of *h*BuChE and the reproduction of the binding mode of the co-crystallized ligand *N*-((1-(2,3-dihydro-1*H*-inden-2-yl)piperidin-3-yl)methyl)-*N*-(2-(dimethylamino)ethyl)-2-naphtamide was considered to estimate the accuracy of the docking program in pose generation [40]. It should be noted that this compound gave a picomolar inhibition constant against *h*BuChE due to strong cation-π interactions and is currently a promising advanced lead compound. A valid metric to reach this goal consists in calculating the Root Mean Square Deviation (RMSD) between the

heavy atoms of the native and the corresponding docking pose. In this case, Glide software was considered to be reliable, since a value lower than 2 Å was obtained (Figure s1) [40].
Docking results corroborated the previous bioassay studies showing that they are *h*BuChE site binders, mainly by π-π interactions. In particular, all of our docked derivatives performed such interaction with Trp82 (Figure 6). The docking poses of such derivatives and that of the co-crystallized ligand were scored using the Molecular Mechanics/Generalized Born Surface Area (MM-GBSA) binding free energy estimation. The experimental inhibition data and the molecular modelling scores (Table 4) were in good agreement, in fact these studies indicated that compound **(1b)** was endowed with the best binding free energy, followed in decreasing order by **(2j)**, **(1a)** and **(2a)**.

Table 4. The ligands target theoretical binding free energy for *h*BuChE (in kcal/mol).

Compound	MM-GBSA
1a	-44.05
1b	-56.19
2a	-43.22
2j	-47.71
X-ray ligand[a]	-71.52

[a] Naphtamide derivative (see above) co-crystallized in the PDB model of BuChE (PDB code: 5NN0)

Regarding the binding modes, the isatin core of compound **(1a)** was orientated towards Trp82 establishing π-π contacts. Meanwhile its phenyl ring was shown to interact with both Phe329 and Trp231. In the most active binder **(1b)**, the replacement of the phenyl ring by the menthol moiety led to a different orienation in the *h*BuChE binding pocket. Compound **(1b)** formed one hydrogen bond with the Thr120 side-chain via the isatin 3-carbonyl sp^2 oxygen and π-π interaction with Trp82 by means of the triazole ring. Comparing the docking pose of **(1a)** with that of **(2a)**, it was noted that the introduction of the oxindole slightly influenced the target recognition. Indeed, similarly to **(1a)**, the triazole phenyl unit of compound **(2a)** was involved in π-π contacts with the Phe329 and Trp231 aromatic residues. Additionally, such binding modes were further stabilized by an H-Bond between the ligand hydroxyl group and Asp70 side chain. In the case of **(2a),** the substitution of the phenyl ring by the menthol unit in **(2j)** induced an opposite orientation of the oxindole moiety which was directed towards Trp231. However, the same π-π interactions observed for **(1a)** and **(2a)** were maintained. These docking studies suggest that our derivatives interact favourably with appropriate *h*BuChE binding pocket residues, and these interactions could play a key role in target recognition and complex stabilisation. It should be noted that although a similar PAS in BuChE to that of AChE is still under investigation [41], there are indications that the aliphatic amino acids, Asp68, Glu119 and Ala277 are found in a comparable area of *h*BuChE and both Asp70 and Try332 are conserved [16b]. With this information in hand, upon observation of Figure 6 there are indications that both **(1a)** and **(2j)** are close to Asp70, in the case of **(1b)** there seems to be an H-Bonding interaction with the triazole unit and in **(2a)** an H-Bonding interaction with the oxindole 3-carbonyl unit.

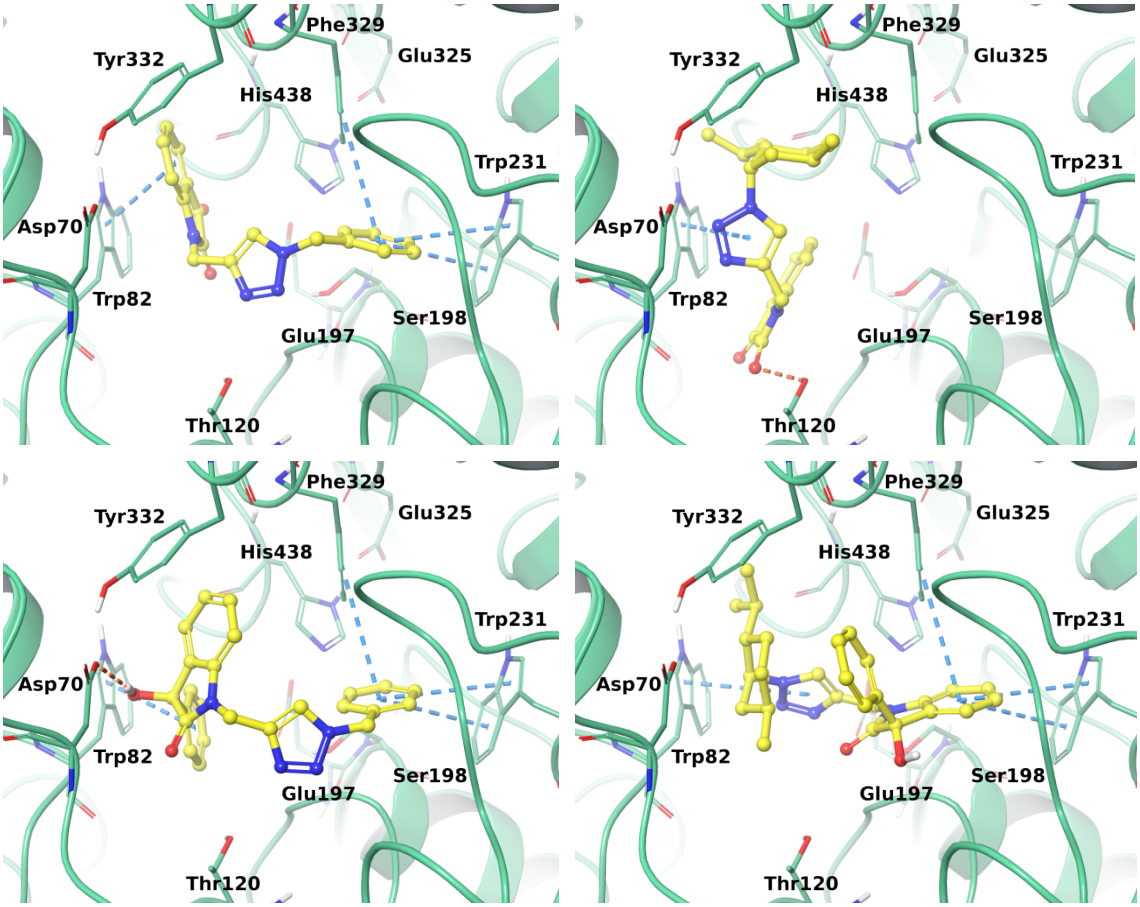

Figure 6. Docking poses of compounds: Top-left **(1a)**, Top-right **(1b)**, Bottom-left **(2a)** and Bottom-right **(2j)** into the *h*BuChE active site. The enzyme is represented in green cartoons, the most relevant interacting residues and the catalytic triad are depicted as thin tubes and the ligands are shown with a yellow ball and stick representation. π-π interactions and hydrogen bonds are represented in light-blue and orange.

In the case of **(1b)** it is quite close to the Tyr332 residue which is also the case with **(2j)**. None of these inhibitors seem to be close to the Phe329 residue, which is a residue that was purported to have a significant role in the formation of the PAS of *h*BuChE [16b]. None the less we have good indications that our inhibitors do reside to some extent in the *h*BuChE so-called PAS.
For comparative purposes, the most promising binding compound **(1b)** was also evaluated against *h*AChE following the same computational protocol. Glide was able to reproduce with fidelity the geometry of the co-crystallized Donepezil (Figure s2). Compound **(1b)**, was shown to establish both π-π interactions with Tyr337/Trp286 and an H-bond with the side chain of Phe295 (which resides in the acyl binding site), but unlike Donepezil (one of the current drugs in clinical use against Alzheimer's disease) it could not interact with the internal Trp86 (Figure 7). The interaction of **(1b)** with Phe295 (which is an amino acid residue in the acyl binding site) indicates that this inhibitor occupies the main gorge of the enzyme. Moreover, the interaction between the Trp286 residue which resides in the PAS and the isatin unit of **(1b)** via π–π stacking was a good indication of binding of this inhibitor to the PAS binding site.

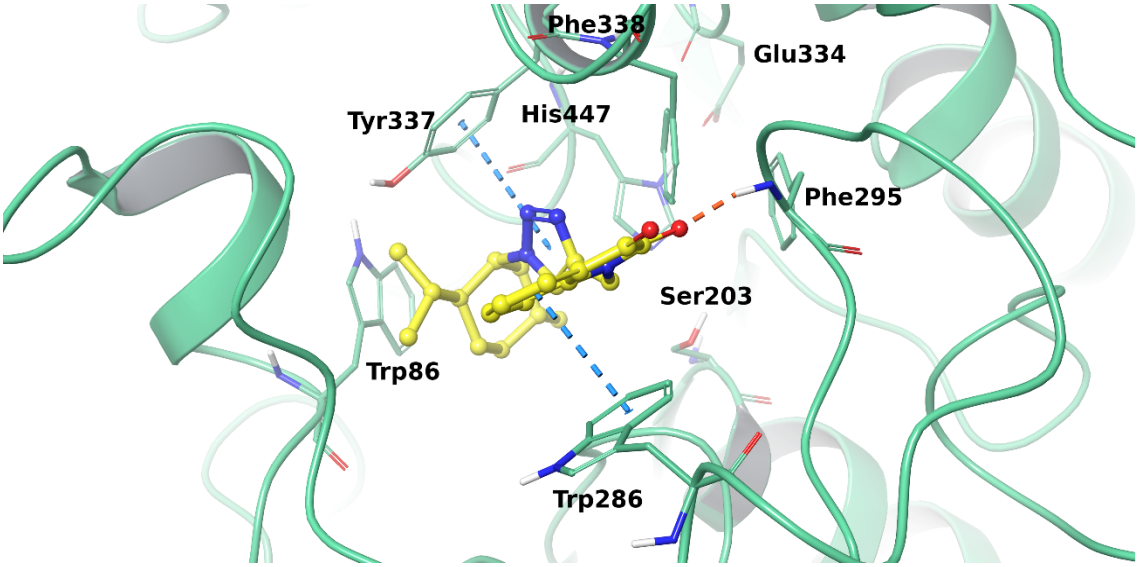

Figure 7. Docking pose of compound **(1b)** into the *h*AChE active site. The enzyme is represented in green cartoons, the most relevant interacting residues and the catalytic triad are depicted as a thin tubes and the ligand is shown as a yellow ball and stick representation. π-π interactions and hydrogen bonds are represented in light-blue and orange.

Our study pursued by exploring the enzymes structural modification and stabilization induced by **(1b)** on *h*AChE and *h*BuChE. Thus, the *h*AChE and *h*BuChE models in apo form and complexed with **(1b)**, were submitted to 100 ns of molecular dynamics (MD) simulations. In fact, if a ligand binding generates strong perturbation of the target conformational properties, the recognition could be energetically penalized or prevented. In particular, in order to evaluate the **(1b)** influence on target stability, for each enzyme the 1,000 MD trajectory frames were aligned to the corresponding starting structure and the RMSD computations of the target not hydrogen atoms were carried out and represented in 2D matrices (Figure 8). The RMSD data highlighted enzyme isoform dependent differences. Actually, the ligand induced a stabilization of the *h*BuChE stronger than *h*AChE as reported by RMSD values wider in the second case with respect to the former one.

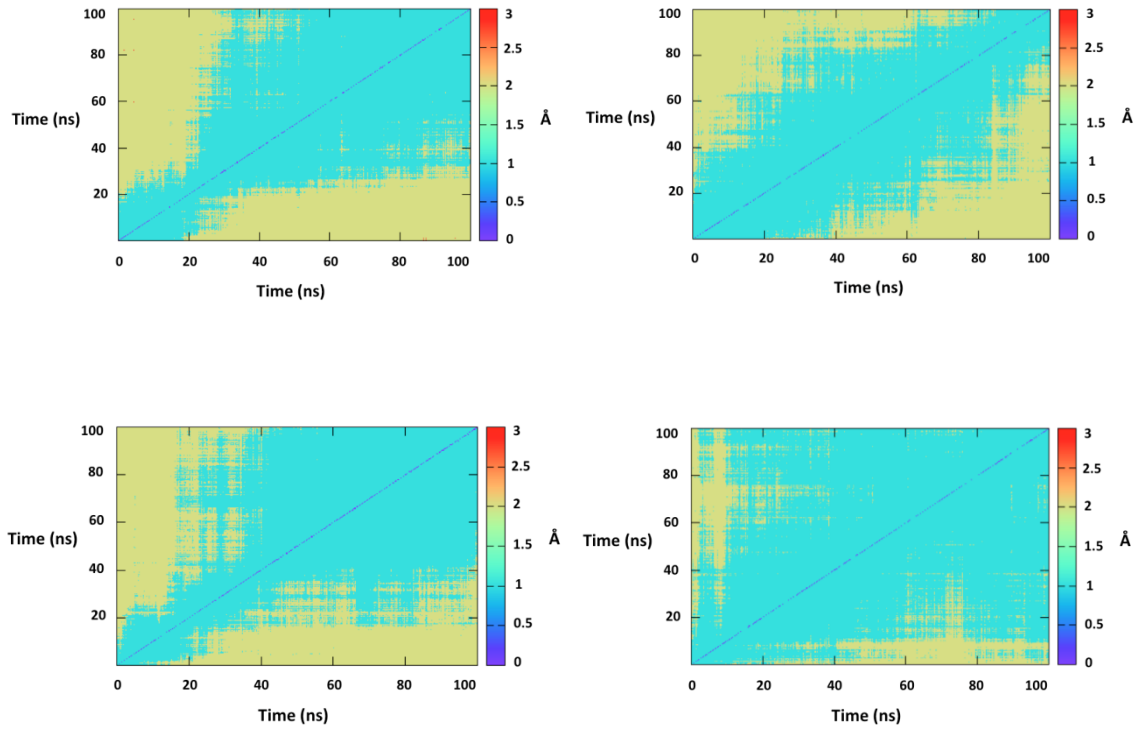

Figure 8. RMSD matrices of Top-left ligand free *h*AChE, Top-right, ligand free *h*BuChE, Bottom-left **(1b)** bound *h*AChE and Botton-right **(1b)** bound *h*BuChE.

2.2.5. STD-NMR studies for accessing BuChE inhibitory activity

Saturation transfer difference NMR (STD-NMR) spectroscopy is a useful technique to study the specific interactions between proteins and ligands in solution [42] and it currently has been recognized as a standard tool for drug discovery in the field AD [42b]. Over the last years STD-NMR spectroscopy has become an important tool for validation of molecular docking studies. The STD-NMR experiment was setup for compound **(1a)** mapping. Unfortunately for solubility issues it was not possible to do the STD-NMR experiment with **(1b)**, and as compound **(1a)** presented better solubility in aqueous solution than **(1b)**, **(1a)** was used in these studies. The STD-NMR experiment was carried out with a 200-fold ligand excess of **(1a)**, this solution was irradiated with various saturation times. In Figure 9 the spectra for the reference mixture (A) and the respective STD with 2s of saturation are presented, the numerical values for the binding epitope of **(1a)** designate the saturation as a percentage, between the ligand protons and the protein active site, normalized to the maximum ligand STD signal (H1, H4; 100%). In the case of the STD-NMR analysis of ligand **(1a)** of ligand **(1a)** (see Fig. 9**)** it was observed that the H1 and H4 protons in the isatin core are saturated to the highest degree, suggesting their interactions by π-π stacking with two amino acids residues, which on the basis of the docking study above in Fig. 6 could be assigned to the Trp82 and Tyr322 residues. Also, the H2 and H3 protons in the isatin core showed 92% and 80% saturation, respectively, probably due to strong interactions with the amino acids residues Trp82 and Tyr322 (which is clearly demonstrated in the docking study (Fig. 6) However, of the two, H2 has highest attenuation probably because of its close proximity to the Tyr322 aromatic unit (see Fig. 9 (a)). The phenyl ring protons (H8, H9, H10, H11 and H12) show high levels of attenuation, which is probably due to close proximity with the Phe329 and Trp231 residues, and interaction via edge-to-face effects [43]. The H6 proton from the triazole ring showed an STD-attenuation of 96%, perhaps due to interaction with the His438 amino acid residue. The H5 methylene protons don't seem to show any interaction with the enzyme, even though the H7 methylene protons showed a weak saturation transfer of 48%. These STD results support the molecular docking studies with **(1a).** While conducting these studies we noticed that when **(1a)** was mixed with the BuChE protein, several of the key resonances seemed to undergo a mild duplication (compared to the ^{1}H NMR spectrum of **(1a)** shown in Fig. s5, Supporting information, there was a second smaller peak to the right of the H6 signal at *ca.* 8.4 ppm and for the H7 and H5 signals at both *ca.* 5.05 and *ca.* 4.80 ppm). We considered this phenomenon to be due inhomogeneities in the sample caused by slight solubility issues with the protein. We also observed similar peak duplication in the case of isatin (see Fig. s6, SI), although this was not observed in the case of (2a) (Fig. s7, SI).

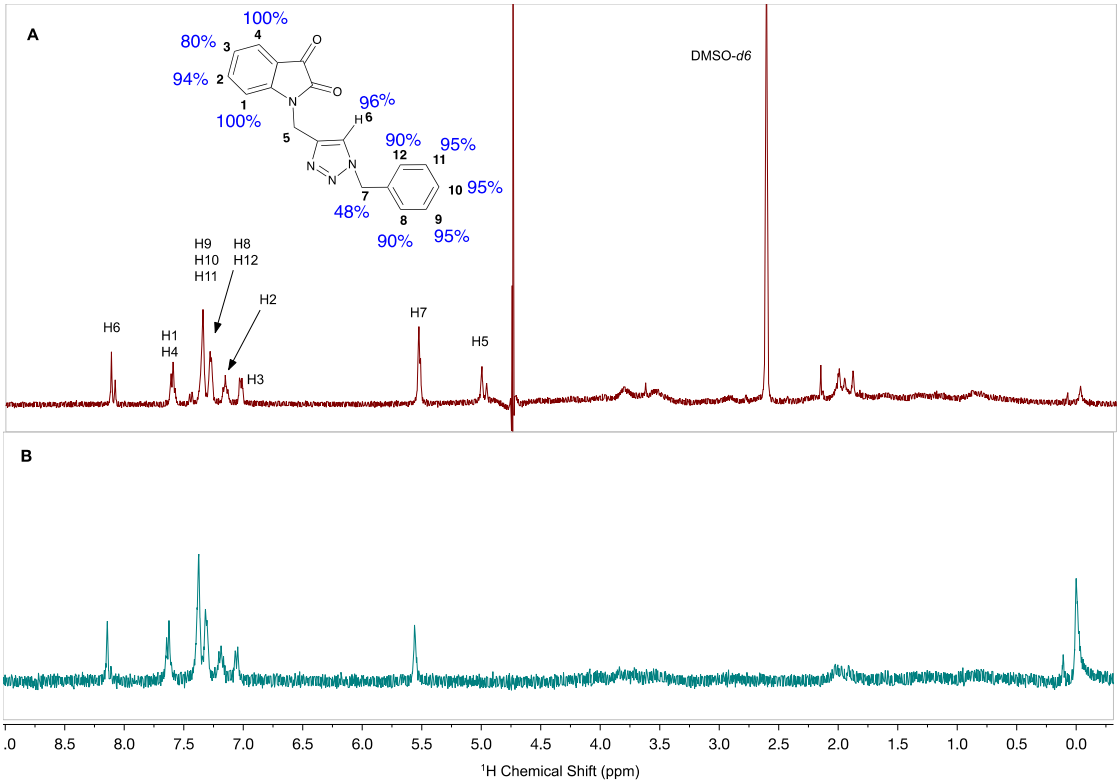

Figure 9. (A) reference ^{1}H NMR spectrum of compound **(1a)** (0.8 mM) with *eq*BuChE enzyme (4µM), **(B)** the corresponding STD-NMR spectrum with 2s of saturation. The protons H1 and H4 were set to 100%. The NMR spectra were recorded at 20 °C.

When Isatin was mixed with BuChE (Fig. s6), there was also the appearance of extra-peaks (in the range 7.3-7.5 ppm) and was probably for the same reason.

2.2.6. Cell-based Screening

2.2.6.1 Hepatotoxicity Studies

Viability profiles of compounds **(1a)**, **(1b)**, **(1c)**, **(2j)** and **(2k)** were performed by using cultured liver cells (human hepatoma cell line HepG2) which were available in our laboratory. The HepG2 cells were exposed to each compound for 24 hours, at increasing concentrations ranging from 0 to 25 µM (*i.e.* 1, 5, 10, 25 µM) in serum-free medium. Cell viability was evaluated after 24 hours exposure by the MTT assay. All compounds were found to be non-toxic on HepG2 (Figure 10), although the compound **(2j)** (purple line) was found to be toxic at the highest concentration (25 µM).

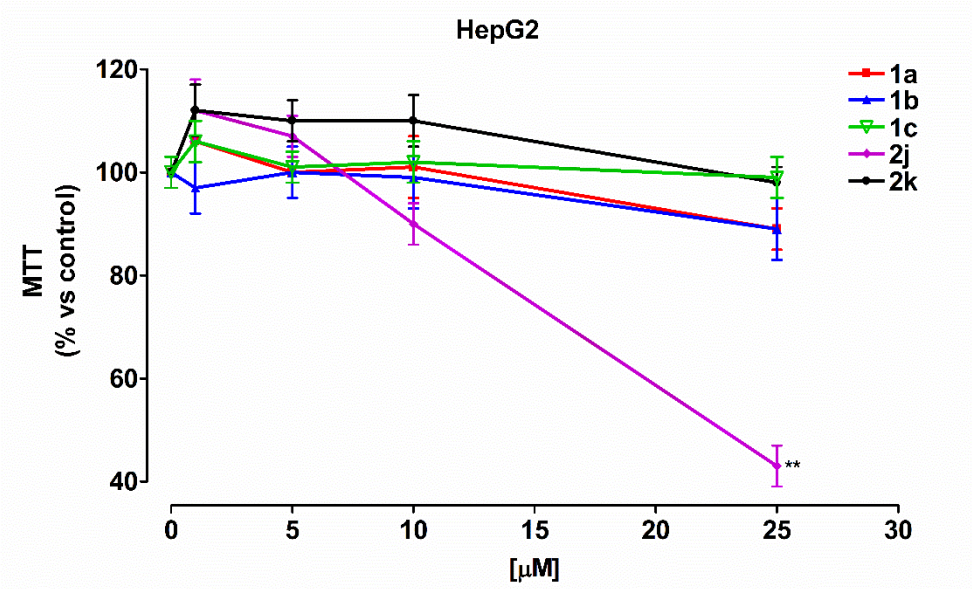

Figure 10. MTT assay for evaluating the hepatotoxicity of **(1a)**, **(1b)**, **(1c)**, **(2j)** and **(2k)** on HepG2 after 24 h treatment. Results are expressed as percentage of control, untreated cells and each point is the mean ± SE of 3 different experiments, each run was conducted in quadruplicate. ** $p < 0.01$ compared to control conditions (0 μM), Bonferroni's test after ANOVA.

2.2.6.2 Neurotoxicity Studies

Furthermore, the neurotoxicity was evaluated on rat primary neurons (Figure 11). As for HepG2, differentiated CGNs were exposed to each compound for 24 hours, at the same concentrations previously used (*i.e.* 1, 5, 10, 25 μM) in serum-free medium and viability was measured by the MTT assay. While **(2j)** (purple line) was toxic even at low concentrations (1 μM), gratifyingly, **(1a)**, **(1b)** and **(1c)** (respectively red, blue and green line) showed neurotoxicity only at high concentrations (25 μM) and **(2k)** (black line) was completely non-neurotoxic.

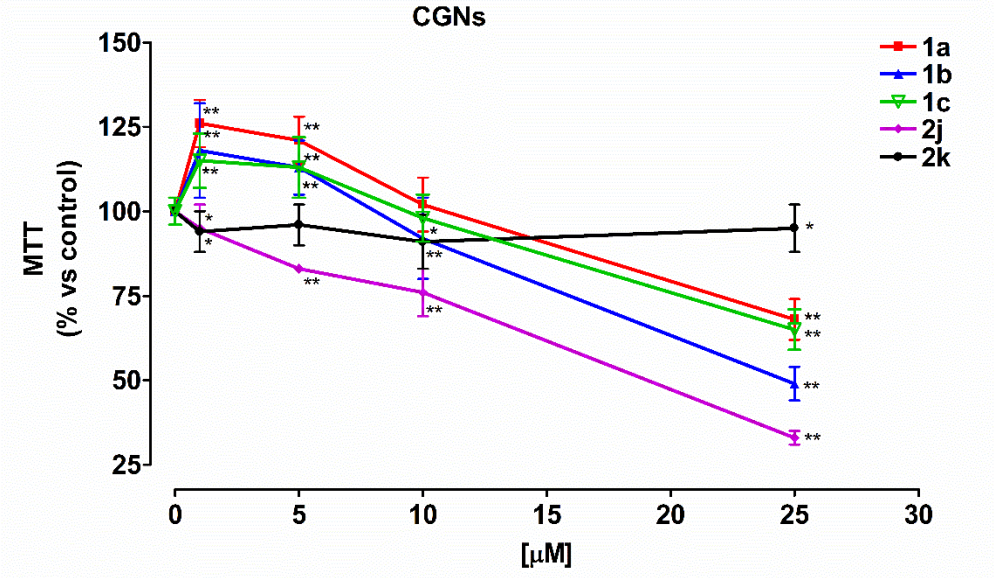

Figure 11. MTT assay for neurotoxicity of **(1a)**, **(1b)**, **(1c)**, **(2j)** and **(2k)** on primary rat CGNs after 24 h treatment. Results are expressed as percentage of controls and each point is the mean ± SE of 3 different experiments, each run-in quadruplicate. * $p < 0.05$, ** $p < 0.01$ compared to control conditions (0 μM) Bonferroni's test after ANOVA.

To confirm the neurotoxicity data of the compounds, a non-metabolic cell death assay was performed. Differentiated CGNs were exposed to each compound at 5 µM for 24 hours in serum-free medium and the viability was evaluated by the counting of healthy, non-condensed/total nuclei after staining with Hoechst dye. No toxicity was observed for all the tested compounds at 5 µM, except for **(1a)** and **(2j)**, which showed a statistically significant decrease of CGNs viability (respectively 85% and 64%).

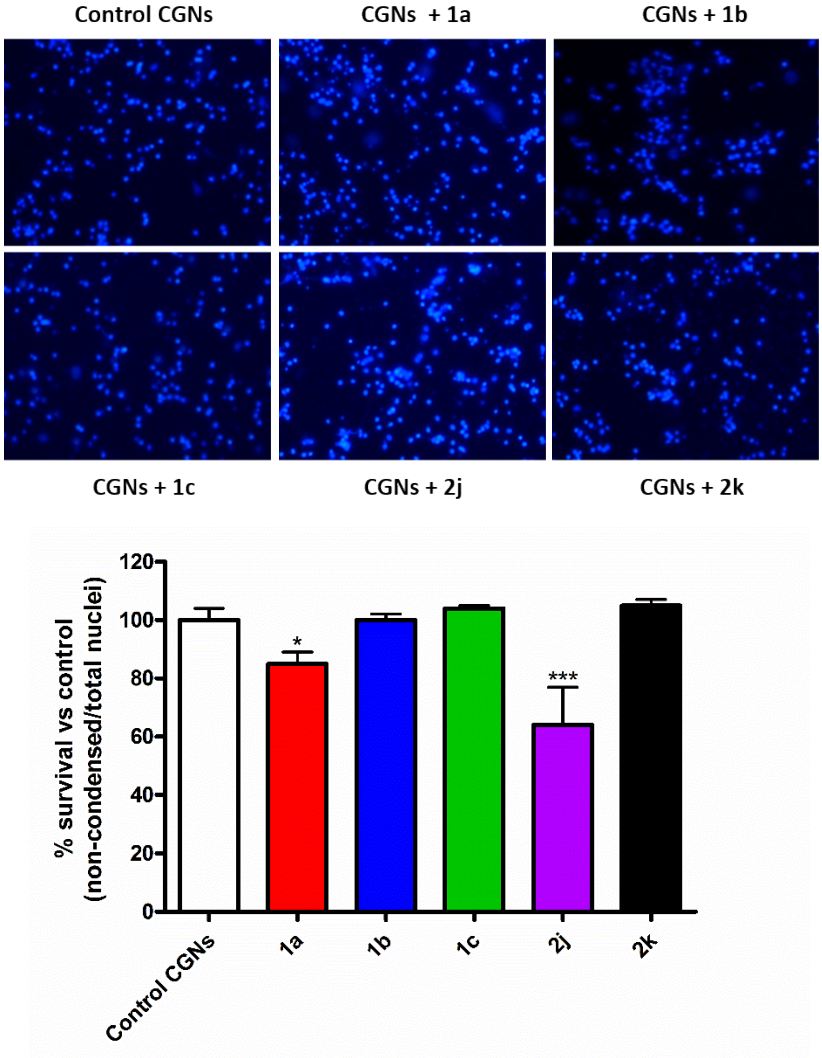

Figure 12. Nuclei counting following Hoechst staining to test the toxicity of the compounds toward differentiated CGNs after 24 h treatment. Results are expressed as percentage of non-condensed nuclei/total nuclei counting following Hoechst staining. Results are the mean ± SE of five images. *p< 0.05 ***p< 0.001 compared to control CGNs, Bonferroni's test after ANOVA.

3. Conclusions

We have described the application of isatin and 3-hydroxyindole-1,2,3-triazole hybrids for AChE, BuChE as well as Aβ anti-aggregation activity, and a study of both their hepatotoxicity and neurotoxicity *in vitro*. Compound **(1b)** – an isatin derivative - was the most potent and selective BuChE inhibitor (IC_{50} = 460 nM with *eq*BuChE and 510 nM in *h*BuChE). In the case of the $A\beta_{42}$ self-aggregation inhibition studies **(1a)** gave the best results. The 3-hydroxyoxindole counterparts were generally less potent, the best was **(2j)** with an IC_{50} of 2.20 µM for *eq*BuChE. Molecular docking studies afforded crucial insights into the mechanism of action of these inhibitors and there

were good indications that regions of the chemical structures of these inhibitors interacted or were located in the PAS of AChE and the corresponding region of BuChE. This has been supported by STD-NMR.
Although the compounds showed only weak anti-Aβ plaque formation, they manifested no hepatotoxicity and with the exception of **(1a)** and **(2j)**), showed low neurotoxicity from both an MTT and a non-metabolic cell death assay on rat primary neurons.

4. Experimental Section

4.1. Synthesis

General remarks: Reagents were obtained from Sigma–Aldrich, Acros, Strem and Alfa Aesar and were used as received. The solvents used were dried using current laboratory techniques [44]. Reactions with transition metals were conducted in a Radley's® 12-position carousel reactor under a nitrogen atmosphere or in round-bottom flasks. Column chromatography was carried out on silica gel (SDS, 0.060-0.200 mm, 60Å). Thin-layer chromatography (TLC) was carried out on aluminum-backed Kieselgel 60 F254 plates (Merck and Machery Nagel). Plates were visualized either by UV light or with phosphomolybdic acid in ethanol. Melting points (m.p.) were determined with a Barnstead Electothermal 9100 apparatus and are uncorrected. NMR spectra were recorded with a Bruker Avance III instrument (400 MHz). Chemical shifts are quoted in parts per million (ppm) relative to δ= 0.0 ppm for tetramethylsilane and were referenced to the appropriate non-deuterated solvent peak. Coupling constants (J) are reported in Hz and refer to apparent peak multiplicities. Splitting patterns are reported as s, singlet; d, doublet; t, triplet; m, multiplet; br, broad.
Low resolution mass spectra (LRMS) were recorded with a quadrupole mass spectrometer Waters ZQ4000 at the Chemistry Department University of Salamanca. The ionization was performed by ESI and the samples were infused in methanol**.** The high-resolution mass spectra (HRMS) were recorded on a Q Exactive mass spectrometer in the chemistry department at the University of Seville (Servicio de Espectrometría de Masas, CITIUS). The syntheses of compounds **(1a-c)** and **(2a-i)** were already reported in literature [36].

4.1.1. *(S)-3-hydroxy-1-((1-((1*S,*2*S,*5*R*)-5-isopropyl-2-methylcyclo hexyl)-1*H*-1,2,3-triazol-4-yl)methyl)-3-phenylindolin-2-one* **(2j)**:

In a Radley's® 12-position carousel reactor under a nitrogen atmosphere was added $[Rh(C_2H_4)_2Cl]_2$ (5.3 mg, 0.0136 mmol, 5 mol%), (R)-BINAP (17 mg, 0.0273 mmol, 10 mol%), *N*-triazole-isatin derivative **(1b)** (100 mg, 0.27 mmol), $PhB(OH)_2$ (67 mg, 0.55 mmol, 2 eq.), K_2CO_3 (113.2 mg, 0.82 mmol, 3 eq.) and toluene (2 mL). The reaction was left stirring at 60ºC for 24 h. After that the solvent was evaporated at reduced pressure and the crude product was purified by silica gel chromatography using a gradient comprising, Hexane/Et_2O (1/1) to (1/2) to Et_2O, affording the desired compound **(2j)** as a foamy white solid, (70.1 mg, 63%) m.p.= 147.2-149.6 ºC. ^{1}H NMR ($CDCl_3$, 400 MHz) δ= 0.69-0.71 (d, *J*= 8.0 Hz, 3H, CH_3), 0.75-0.77 (d, *J*= 8.0 Hz, 3H, CH_3), 0.83-0.85 (d, *J*= 8.0 Hz, 3H, CH_3), 0.98-1.04 (m, 2H, CH_2 + CH), 1.25-1.43 (m, 2H, CH_2 + CH), 1.56-1.63 (m, 1H, CH_2 + CH), 1.66-1.78 (m, 1H, CH_2 + CH), 1.80-1.91 (m, 3H, CH_2 + CH), 3.54 (s br, 1H, OH), 4.91-5.10 (m, 3H, CH_2 + CH), 7.04-7.08 (t, *J*= 8 Hz, 1H, Ar), 7.21-7.25 (m, 2H, Ar), 7.28-7.35 (m, 6H, Ar), 7.57 (s, 1H, CH). ^{13}C NMR ($CDCl_3$, 100 MHz) δ= 20.5, 21.2, 22.4, 24.8-

24.9, 26.4-26.5, 29.2, 34.6, 35.8,35.9, 40.7, 46.7,46.8, 59.5, 59.6, 78.1, 110.4, 123.6, 123.8, 125, 125.4, 128.5, 128.7, 130.2, 131.5, 140.2, 141.6, 142.3, 177.3. MS (ESI) m/z: 445.23 $[M+H]^+$, HRMS 467.2417, $C_{27}H_{32}N_4NaO_2$ requires 467.2423.

4.1.2. *1-((1-((1*S*,2*S*,5*R*)-5-isopropyl-2-methylcyclohexyl)-1*H*-1,2,3-triazol-4-yl)methyl)spiro[indoline-3,2'-[1,3]dioxolan]-2-one* **(2k)***:*

A mixture of compound **(1b)** (100 mg, 0.27 mmol), ethylene glycol (0.3 mL, 5.5 mmol, 20 equiv.) and *p*-TsOH (3 mg, 0.0136 mmol, 5 mol%) in toluene (10 mL) was refluxed overnight. The solvent was then evaporated under reduced pressure. To the crude product was added CH_2Cl_2 and washed with a sat. aq. solution of $NaHCO_3$. The aqueous phase was extracted with CH_2Cl_2. The organic phases were dried with $MgSO_4$, filtered and the solvent evaporated under reduced pressure. The crude product was purified by silica gel chromatography using the following gradient (Hexane/AcOEt (5/1) to (2/1) to (1/1)), affording the desired compound **(2k)** as a foamy white solid (90 mg, 79%). m.p.= 165.2-167.7 ºC. ^{1}H NMR ($CDCl_3$, 400 MHz) δ= 0.70-0.72 (d, *J*= 8.0 Hz, 3H, CH_3), 0.76-0.78 (d, *J*= 8.0 Hz, 3H, CH_3), 0.83-0.84 (d, *J*= 8.0 Hz, 3H, CH_3), 0.97-1.04 (m, 2H, CH_2 + CH), 1.29-1.44 (m, 2H, CH_2 + CH), 1.62-1.78 (m, 2H, CH_2 + CH), 1.88-1.92 (m, 3H, CH_2 + CH), 4.29-4.37 (m, 2H, CH_2), 4.55-4.63 (m, 2H, CH_2), 4.88-4.96 (m, 3H, CH_2 + CH), 7.05-7.08 (m, 1H, Ar), 7.15-7.17 (d, *J*= 8 Hz, 1H, Ar), 7.31-7.35 (m, 2H, Ar), 7.54 (s, 1H, CH). ^{13}C NMR ($CDCl_3$, 100 MHz) δ= 20.5, 21.2, 22.3, 24.9, 26.4, 29.1, 34.7, 35.5, 40.7, 46.9, 59.6, 66.00, 102.4, 110.5, 123.6, 123.8, 123.9, 124.7, 131.9, 141.3, 143.6, 173.2. MS (ESI) m/z: 411.25 $[M+1]^+$, HRMS 433.2210, $C_{23}H_{30}N_4NaO_3$ requires 433.2216.

4.2. Cholinesterase evaluation assay

Enzymatic activity of *electrophorus electricus* AChE and BuChE from equine serum was evaluated using the Ellman's cholorimetric assay, with minor modifications [45]. DMSO (1.25% final concentration in cuvette) was used for preparing the stock inhibitor solutions. Enzymatic kinetics were monitored by UV-Vis spectroscopy using DTNB (5,5'-dithiobis(2-nitrobenzoic acid), 0.875 mM) as the chromogenic agent. Reaction took place in a buffered medium (0.1 M phosphate buffer, pH 8.0), T = 25ºC, being monitored for 125 s.

For determining the percentage of inhibition ([I] = 100µM), the substrate concentration (acetylthiocholine iodide for AChE; *S*-butyrylthiocholine iodide for BuChE) was fixed at 452 µM.

Cornish-Bowden plot (1/V *vs.* [I] and [S]/V *vs.* [I]) was used for estimating the inhibition constants (K_i's) and the mode of action

Statistics

Data are expressed as the mean ± SD; independent experiments are conducted in duplicate.

Studies on *h*BuChE

DTNB (Ellman's reagent) and BTC iodides were purchased from Sigma-Aldrich (Steinheim, Germany). *h*BuChE (E.C. 3.1.1.8, from human plasma) was kindly donated by Dr. Oksana Lockridge, Nebraska Medical Centre. Inhibitors were dissolved in DMSO at a concentration of 3.33

mM (100 µM in the assay) and diluted in steps to 3.33 nM (0.1 nM in the assay). The assay buffer was prepared from potassium dihydrogen phosphate (3.12 g in 500 mL of bidistilled water) and pH value was adjusted to pH = 8.0 with 0.1 M NaOH solution. BuChE was dissolved in assay buffer, stabilized with 1 mg/mL bovine serum albumin (Sigma-Aldrich, Steinheim, Germany), and stored at 7 C until usage. A solution of 5,5´-Dithiobis-(2-nitrobenzoic acid) in buffer at 10 mM (0.3 mM in the assay) was prepared. The substrate butyrylthiocholine was dissolved in assay buffer to 75 mM (452 µM in the assay) and kept frozen until usage. The absorbance of probes was measured with a Shimadzu UVmini-1240 spectrometer (Shimadzu, Kyoto, Japan) at 412 nm.

IC_{50} Determination

The assay was carried out at room temperature (25°C). 900 µL of the buffer, 30 µL of 5,5´-dithiobis-(2-nitrobenzoic acid) solution (10 mM, 0.3 mM in the assay) and 30 µL of enzyme solution (*h*BChE, 2.5 units/mL) were mixed in a cuvette. Then, 30 µL of inhibitor solutions with different concentrations were added and the solutions were mixed. After 5 min incubation, 6 µL of substrate solution (butyrylcholine; 75 mM, 452 µM in the assay) were added. The mixture was left to allow substrate hydrolysis for 2.5 min. Then, the absorbance was measured at λ = 412 nm to quantify the quantity of thiols formed, whereas enzyme activity was determined 3 times for every concentration with at least 7 different concentrations. A blank value was determined by replacing the enzyme solution with buffer. The compound solution was replaced with DMSO. The maximum enzyme activity was determined with 30 µL of DMSO instead of the compound solution which did not affect enzyme activity. The enzyme activity in percent of maximum activity was calculated and plotted against the logarithmic inhibitor concentration, from which IC_{50} values were calculated with the software GraphPad Prism 5.

4.3 Inhibition of Aβ_{42} Self-Aggregation.

As reported in the previously published protocol by Bartolini *et al.* [46a] HFIP pretreated Aβ_{42} samples (Bachem AG, Switzerland) were solubilized with a CH_3CN/0.3 mM Na_2CO_3/250 mM NaOH (48.4:48.4:3.2) mixture to obtain a 500 µM stock solution. Experiments were performed by diluting (final Aβ concentration 50 µM) and incubating the peptide in 10 mM phosphate buffer (pH = 8.0) containing 10 mM NaCl, at 30 °C for 24 h with and without inhibitor (50 µM, Aβ/inhibitor = 1/1). Blanks containing the tested inhibitors were also prepared. To quantify amyloid fibril formation, the thioflavin T fluorescence method was used [46b]. After incubation, samples were diluted to a final volume of 2.0 mL with 50 mM glycine–NaOH buffer (pH 8.5) containing 1.5 µM thioflavin T. A 300-second-time scan of fluorescence intensity was carried out (λ_{exc} = 446 nm; λ_{em} = 490 nm, FP-6200 fluorometer, Jasco Europe), and values at plateau were averaged after subtracting the background fluorescence of 1.5 µM thioflavin T solution. The fluorescence

intensities obtained in the absence and in the presence of tested inhibitors were compared and the percent inhibition due to the presence of the inhibitor was calculated by the following formula: $100 - (IF_i/IF_o \times 100)$ where IF_i and IF_o are the fluorescence intensities obtained for $A\beta_{42}$ in the presence and in the absence of inhibitor, respectively.

4.4 Cell based assays

4.4.1 Hepatotoxicity

To evaluate the hepatotoxicity of the compounds, human hepatoma cell line (HepG2) which was available in our laboratory was used. Cells were cultured in Dulbecco Modified Eagle Medium (DMEM) supplemented with 10% heat inactivated Fetal Bovine Serum (FBS), 1% Penicillin/Streptomycin and 2mM glutamine (all reagents were from Aurogene, beside glutamine, which was from Sigma-Aldrich) at 37 C in a humidified atmosphere containing 5% CO_2. Cells were plated on 96 well plates, previously coated with 10 µg/mL poly-L-lysine (Sigma-Aldrich) at the density of 2.5 x 10^4/well and treated with increasing concentrations of the compounds (ranging from 0 to 25 µM), in serum-free DMEM for 24 hours.

Primary cultures of cerebellar granule neurons (CGNs) were used to evaluate neurotoxicity of the compounds. CGNs were prepared from 7-day-old Wistar rats [47]. Animals were bred at the University of Bologna with *ad libitum* food and water in a 12/12 hour light-dark cycle at temperature (20 °C ± 2 C) and humidity-controlled (55 ± 5%). The health state of mice was periodically controlled by veterinarians. The experiments were conducted in accordance with Italian and European Community laws (Directive 2010/63/EU).

CGNs were isolated from cerebella and were plated on 96-well plates at the density of 1.2×10^5 cells/well in BME (Aurogene) supplemented with 10% heat-inactivated Fetal Bovine Serum (FBS, Aurogene), 2 mM glutamine (Sigma-Aldrich), 100 µM gentamicin sulfate (Sigma-Aldrich), and 25 mM KCl (Sigma-Aldrich). To avoid glial proliferation, 10 µM cytosine arabino-furanoside (Sigma-Aldrich) was added 16 hours after plating. After 7 days *in vitro*, differentiated CGNs were treated with the selected compounds at different concentrations (ranging from 0 to 25 µM) in serum-free medium for 24 hours.

4.4.2 MTT Assay

Cell viability was measured by MTT assay after 24 hours of treatment. Thiazolyl blue (0.1 mg/mL; Sigma-Aldrich) was added to the culture medium. Following a 30-minute incubation time for HepG2 and 20 minutes for CGNs at 37 °C in the dark, the precipitate was dissolved in 0.1 M Tris-HCl pH 7.5 containing 5% Triton X-100 (all from Sigma-Aldrich) in agitation. The absorbance was read at 570 nm using a multiplate spectrophotometric reader (Bio-Rad Microplate reader BenchMark).

Values are the mean ± SE of 3 independent experiments performed in quadruplicate. Statistical analysis was perfomed using GraphPad Prism 4 software (one-way ANOVA followed by Bonferroni post-hoc comparison test); p values less than 0.05 were considered statistically significant.

4.4.3 Nuclei Counting after Hoechst Staining

Differentiated CGNs were exposed to each compound at 5 μM for 24 hours. Cells were fixed for 20 minutes with 4% PFA in phosphate buffer, washed in PBS and incubated with 0.1 μg/mL of Hoechst 33258 (Sigma-Aldrich) for 5 minutes at room temperature. By using a fluorescence microscope (20× objective; Nikon Eclipse TE 2000-S microscope, equipped with an AxioCam MRm digital camera) five randomly fields were acquired from each sample. The healthy/total nuclei were counted by using the manual cell counter plugin of Fiji ImageJ2 software. Neuronal survival was expressed as percentage of non-condensed nuclei on the total nuclei number. Values are the mean ± SE of 5 different images. Statistical analysis was perfomed using GraphPad Prism 4 software (one-way ANOVA followed by Bonferroni post-hoc comparison test); p values less than 0.05 were considered statistically significant.

4.5. Docking Studies

All molecular modelling simulations were carried out using the Schrödinger Suite 2018-1 [48] and OPLS-A_2005 [49] as force field. The three-dimensional structures of our derivatives were built by using Maestro GUI [50] and the protonation states at physiological pH were evaluated by means LigPrep [51] tool. The Protein Data Bank (PDB) [55] crystallographic entries 4EY7 [52] and 5NN0 [53] were used as receptor models for *h*AChE and *h*BuChE, respectively. Such models were selected taking into account the resolution, the absence of mutations in the active sites, the availability of co-crystalized reversible ligands. The original PDB structures were adjusted, employing the Protein Preparation Wizard too [54] by adding hydrogen atoms, removing co-crystallised water molecules and fixing missing residues. Docking experiments were computed by means of Glide [55] software applying the standard precision (SP) method and the ligand flexible algorithm. The binding free energy was estimated by the MM-GBSA method accounting for the receptor and ligand conformational changes needed to form the complex. Solvent effects were mimicked by the VSGB 2.0 [56] continuum dielectric model, as implemented in Prime [57]. The *h*ChEs targets active sites were defined by a regular grid box of 27,000 $Å^3$ centred on the catalytic serine residues. Best docking complexes of targets and **(1b)** were considered as starting structure for molecular dynamics investigation carried out using Desmond [58] software. The SPC explicit solvent model was applied for generating solvated systems. The overall electrostatic net charge was neutralized including Na^+ ions into the *h*AChE systems and Cl^- ions into the *h*BuChE ones.

The default Desmond protocol was applied for equilibrating solvated systems. The production run of MD simulations was carried out at 300 K, up to 100 ns, with an integration time step equal to 2 fs. MD frames were sampled at regular time intervals equal to 100 ps collecting 1,000 frames for each simulation.

4.6. STD-NMR

All reagents were obtained from Sigma-Aldrich. *eq*BuChE enzyme used in the STD-NMR experiments was from equine serum (lyophilized powder with phosphate buffer salts, ≥10 units/mg protein). The STD-NMR spectroscopy experiments were performed on a Bruker Avance III 400 MHz HD spectrometer equipped with a 5 mm broadband (PABBO BB/19F-1H/D Z-GRD) resonance probe head. STD-NMR experiments were carried out with solvent suppression and a 10 ms spin-lock filter after the 90° pulse to reduce residual signals from the protein. For selective saturation, cascades of Gaussian pulses with a length of 50 ms and 40 - 60 dB of attenuation were employed, with an interpulse delay of 1 ms [42d]. The on-resonance and off-resonance frequencies were set to 0 and 12000 Hz, respectively. STD-NMR controls were performed using the ligand itself. Blank experiments were performed to guarantee the absence of direct saturation of the ligand proton signals. The relaxation delay was properly adjusted so that the experiment time length was kept constant at 6.5 s. Water suppression at 1880 Hz (4.7 ppm) was conducted. A sweep-width of 8012.82 Hz (20.03 ppm) was employed. The saturation times to obtain the STD epitope mapping were recorded at 0.25, 0.5, 1, 2, 3, 4, and 5 s [23b]. STD spectrum was obtained by subtraction of saturated spectrum from the reference spectrum. STD intensity of individual signal was measured relative to the corresponding signal intensity in the reference spectrum. The stock solution of *eq*BuChE was prepared in D_2O with 5 μM of concentration. A stock solution of compound **1a** (ligand) was prepared in dmso-d_6 with 5 mM of concentration. The sample for STD-NMR analysis was prepared by adding 100 μL of the solution stock of compound **1a** to a 500 μL of *eq*BuChE enzyme solution.

Acknowledgments

We acknowledge the Fundação para a Ciência e a Tecnologia (FCT) for funding through the strategic project Pest-OE/QUI/UI0619/2019, including a post-doc grant to C.S.M. (SFRH/BPD/92394/2013). O.L. thanks the Dirección General de Investigación of Spain (CTQ2016-78703-P), the Junta de Andalucía (FQM134), and the European Regional Development Fund (FEDER) for financial support. We are extremely grateful to COST action 15135, *Multi-target paradigm for innovative ligand identification in the drug discovery process* (MuTaLig). M. Decker acknowledges the German Research Council (Deutsche Forschungsgemeinschaft) under DFG DE 1546/6-3.

Supplementary data

Supplementary data to this article can be found online at https://doi.org/….

References

[1]. P. Csermely, V. Ágoston, S. Pongor, *Trends Pharm. Sci.* 26 (2005) 178-182.

[2]. G. R. Zimmermann, J. Lehár, C. T. Keith, *Drug Discov. Today* 12 (2007) 34-42.

[3]. R. R. Ramsay, M. R. Popovic-Nokolic, K. Nikolic, E. Uliassi, M. L. Bolognesi, *Clin. Trans. Med.* 7:3 (2018).

[4] P. Paudel, S.H. Seong, Y. Zhou, H. J. Park, H.A. Jung, J.S. Choi, *ACS Omega,* 4 (2019) 12259-12270.

[5] R.T. Bartus, R.L.Dean B, Beer, A.S. Lippa, *Science*, 217 (1982) 408–417.

[6] For key publications on AChE see: (a) X. Cousin, T. Hotelier, P. Liévin, J.P. Toutant, A. Chatonnet, *Nucleic Acids Res.* 24 (1996) 132-136. (b) H. Dvir, I. Silman, M. Harel, T.L. Rosenberry, J.L. Sussman, *Chemico-Biol. Int.* 187 (2010) 10-22. For key publications on BuChE see: (a) B. Brus, U. Košak, S. Turk, A. Pišlar, N. Coquelle, J. Kos, J. Stojan, J.-P. Colletier, S. Gobec, *J. Med. Chem.* 57 (2014) 8167-8179. (b) Y. Nicolet, O. Lockridge, P. Masson, J.C. Fontecilla-Camps, F. Nachon, *J. Biol. Chem.* 278 (2003) 41141-41147. (c) F. Nachon, O.A. Asojo, E.O. Borgstahl, P. Masson, O. Lockridge, *Biochemistry* 44 (2005) 1154-1162.

[7] R. Purgatorio, M. de Candia, M. Catto, A. Carrieri, L. Pisani, A. De Palma, M. Toma, O.A. Ivanova, L.G. Voskressensky, C.D. Altomare, *Eur. J. Med. Chem.* 177 (2019) 414-424.

[8] C.I. Wright, C. Geula, M.M. Mesulam, *Ann. Neurol.,* 34 (1993) 373-384.

[9] (a) N.C. Inestrosa, A. Alvarez, C.A. Perez, R.D. Moreno, M. Vicente, C. Linker, O.I. Casanueva, C. Soto, J. Garrido, *Neuron,* 16 (1996) 881-891.

[10] N.C. Inestrosa, M.C. Dinamarca, A. Alvarez, *FEBS*, 275 (2008) 625-632

[11] (a) M. Bartolini, C. Bertucci, V. Cavrini, V. Andrisamo, *Biochem. Pharm*. 65 (2003) 407-416. (b) M.L. Bolognesi, V. Andrisano, M. Bartolini, R. Banzi, C. Melchiorre, *J. Med. Chem.* 48 (2005) 24-27.

[12] N. H. Greig, T. Utsuki, Q.-S. Yu, X. Zhu, H. W. Holloway, T. Perry, B. Lee, D. K. Ingram, D. K. Lahiri, *Curr. Med. Res. Opinion* 17 (2001) 159-165.

[13] S. Diamant, E. Podoly, A. Friedler, H. Ligumsky, O. Livnah, H. Soreq, *Proc. Nat. Acad. Sci.* 103 (2006) 8628-8633.

[14] N.H. Greig, T. Utsuki, D.K. Ingram, Y. Wang, G. Pepeu, C. Scali, Q-S. Yu, J. Mamczarz, H.W. Holloway, T. Giordano, D. Chen, K. Furukawa, K. Sambamurti, A. Brossi, D.K. Lahiri, *Proc. Nat. Acad. Sci.* 102 (2005) 17213-17218.

[15] A.L. Guillozer, J.F. Smiley, D.C. Mash, M.-M. Mesulam, *Ann. Neurol*. 42 (1997) 909-918.

[16] (a) R. Kumar, A. Nordberg, T. Darreh-Shori, *Brain*, 139 (2016) 174-192. (b) M. Hoffmann, C. Stiller, E. Endres, M. Scheiner, S. Gunesch, C. Sotriffer, T. Maurice, M. Decker, *J. Med. Chem.* 62 (2019) 9116-9140.

[16] M. Kaur, M. Singh, N. Chadha, O. Silakari, *Eur. J. Med. Chem.* 123 (2016) 858-894.

[17] M. Kaur, *Key Heterocycle Cores for Designing Multitargeting Molecules* - Chapter 6, U. Silakari (ed.), (2018) 211-246.

[19] P. Brandão, A. J. Burke, *Tetrahedron* 74 (2018) 4927-4957.

[20] (a) M. A. Ali, R. Ismail, T. S. Choon, Y. K. Yoon, A. C. Wei, S. Pandian, R. S. Kumar, H. Osman, E. Manogaran, *Bioorg. Med. Chem. Lett.* 20 (2010) 7064-7066. (b) M. A. Ali, R. Ismail, T.

S. Choon, R. S. Kumar, H. Osman, N. Arumugam, A. I. Almansour, K. Elumalai, A. Singh, *Bioorg. Med. Chem. Lett.* 22 (2012) 508-511.
[21] Y. Kia, H. Osman, R. S. Kumar, V. Murugaiyah, A. Basiri, S. Perumal, H. A. Wahab, C. S. Bing, *Bioorg. Med. Chem.* 21 (2013) 1696-1707.
[22] (a) A. M. Srour, D. H. Dawood, M. N. A. Khalil, Z. M. Nofal, *Bioorg. Chem.* 83 (2019) 226-234. (b) H. Akrami, B. F. Mirjalili, M. Khoobi, H. Nadri, A. Moradi, A. Sakhteman, S. Emami, A. Foroumadi, A. Shafiee, *Eur. J. Med. Chem*. 84 (2014) 375-381.
[23] (a) J. Totobenazara, P. Bacalhau, A. A. San Juan, C. S. Marques, L. Fernandes, A. Goth, A.T. Caldeira, M.R. Martins, A.J. Burke, *ChemistrySelect,* 1 (2016)*,* 3580–3588. (b) P. Bacalhau, L. Fernandes, F. Candeias, E. Carreiro, Ó. López, R. Guedes, T. Caldeira, R. Martins, A.J. Burke, *Bioorg. Med. Chem.,* 27 (2019) 354-363.
[24] A.E. Medvedev, O.A. Buneeva, A.T. Kopylov, O.V. Gnedenko, M.V. Medvedeva, S.A. Kozin, A.S. Ivanov, V.G. Zgoda, A. A. Makarov. *Int. J. Mol. Sci.,* 16 (2015) 476–495.
[25] (a) F. Campagna, M. Catto, R. Purgatorio, C.D. Altomare, A. Carotti, A. De Stradis, G. Palazzo, Eur. J. Med. Chem. 46 (2011) 275-284. (b) R. Purgatorio, M. de Candia, A. De Palma, F. De Santis, L. Pisani, F. Campagna, S. Cellamare, C.D. Altomare, M. Catto, *Molecules,* 23 (2018) 1544 (1-23).
[26] (a) H. Shao, Z. Mi, W.-g. Ji, C.h. Zhang, T. Zhang, S.-c. Ren, Z.-r. Zhu, *Neurochem. Res.* 40 (2015) 2365-2373. (b) Y.-F. Xian, Z.-X. Lin, Q-Q. Mao, S.-P. Ip, Z.-R. Su, X.-P. Lai, *Cell Mol. Neurobiol.* 32 (2012) 353-360.
[27] D. Dheer, V. Singh, R. Shankar, *Bioorg. Chem.* 71 (2017) 30-54.
[28] S. G. Agalave, S. R. Maujan, V. S. Pore. *Chem. Asian J.* 6 (2011) 2696-2718.
[29] K. Bozorov, J. Zhao, H.A. Aisa, *Bioorg. Med. Chem*. 27 (2019) 3511-3531.
[30] G. Wu, Y. Gao, D. Kang, *MedChemComm*, 9 (2018) 149–159.
[31] W. Wang, W. Wang, G. Yao, Q. Ren, D. Wang, Z. Wang, P. Liu, P. Gao, Y. Zhang, S. Wang, S. Song, *Eur. J. Med. Chem*. 151 (2018) 351-362.
[32] (a) G. Smith, M. Glaser, M. Perumal, Q.-D. Nguyen, B. Shan, E. Årstad, E. O. Aboagye, *J. Med. Chem.* 51 (2008) 8057-8067. (b) Q.-D. Nguyen, G. Smith, M. Glaser, M. Perumal, E. Årstad, E. O. Aboagye, *Proc*. *Nat. Acad. Sci.* 106 (2009) 16375-16380.
[33] W. Chu, J. Rothfuss, D. Zhou, R. H. Mach, *Bioorg. Med. Chem. Lett.* 21 (2011) 2192-2197.
[34] A. Nagarsenkar, L. Guntuku, S. D. Guggilapu, D. Bai K., S. Gannoju, V. G. M. Naidu, N. B. Bathini, *Eur. J. Med. Chem.* 124 (2016) 782-793.
[35] A. Singh, G. Fong, J. Liu, Y.-H. Wu, K. Chang, W. Park, J. Kim, C. Tam, L. W. Cheng, K. M. Land, V. Kumar, *ACS Omega* 3 (2018) 5808-5813.
[36] C. S. Marques, A. J. Burke, *ChemCatChem* 8 (2016) 3518-3526. C.S. Marques, N. Busto, E. Gaudio, F. Bertoni, A. J. Burke, *Novel N-(1,2,3-Triazolmethyl)Isatin and N-(1,2,3-Triazolmethyl)-3-Hydroxy-3-aryloxindoles with Cytotoxic and Anti-Tumor Activity,* EP3400938, 27-4-2018.
[37] (a) B. N. M. Silva, A. C. Pinto, F. C. Silva, V. F. Ferreira, B. V. Silva, *J. Braz. Chem. Soc.*, 27 (2016) 2378-2382. (b) G. C. Montes, B. N. M. da Silva, B. Rezende, R. T. Sudo, V. F. Ferreira, F. de C. da Silva, A. da C. Pinto, B. V. da Silva, G. Zapata-Sudo, *Molecules*, 22 (2017) 800.
[38] M. S. Poslusney, B. J. Melancon, P. R. Gentry, D. J. Sheffler, T. M. Bridges, T. J. Utley, J. S. Daniels, C. M. Niswender, P. J. Conn, C. W. Lindsley, M. R. Wood, *Bioorg. Med. Chem. Lett.* 23 (2013) 1860-1864.
[39] (a) D. M. Mann, T. Iwatsubo, Y. Ihara, N. J. Cairns, P. L. Lantos, N. Bogdanovic, L. Lannfelt, B. Winblad, M. L. Maat-Schieman, and M. N. Rossor, *Am J. Pathol.* 148 (1996) 1257–1266. (b) M. P. Murphy, H. LeVine, III, J. Alzheimers Dis. 19 (2010) 311-323.

[40] U. Košak, B. Brus, D. Knez, S. Žakelj, J. Trontelj, A. Pišlar, R. Šink, M. Jukič, M. Živin, A. Podkowa, F. Nachon, X. Brazzolotto, J. Stojan, J. Kos, N. Coquelle, K. Sałat, J.-P. Colletier, S. Gobec, *J. Med. Chem.*, 61 (2018) 119-39.
[41] S. Darvesh, M.K. Cash, G.A. Reid, E. Martin, A. Mitnitski, C. Geula, *J. Neuropathol. Exp. Neurol.* 71 (2012) 2-14.
[42] (a) J. Angulo, P. M. Nieto, *Eur Biophys J.* 40 (2011) 1357-1369. (b) B. Meyer, T. Peters, *Angew Chem Int. Ed.* 42 (2003) 864-890. (b) A. De Simone, M. Naldi, D. Tedesco, M. Bartolini, L. Davini, V. Andrisano, *J. Pharm. Biomed*. *Anal.*178 (2020) 112899(1-19). (c) M. Mayer, B. Meyer, *Angew Chem Int Ed.* 38 (1999) 1784-1788. (d) S. Berger, S. Braun, *200 and More NMR Experiments - A Practical Course.* 2014.
[43] M. Nishio, M. Hirota, Y. Umezawa, The CH/P interaction: Evidence, Nature and Consequences, Wiley -VCH, 1998, New York.
[44] W. L. F. Amarego, D. D. Perrin, *Purification of Laboratory Chemicals*, 4th Ed., Butterworth Heinemann, Oxford, UK (1996).
[45] G.L. Ellman, K.D. Courtney, V. Andres Jr., R.M. Featherston, *Biochem. Pharmacol.*, 7 (1961) 88-95.
[46] (a) M. Bartolini, C. Bertucci, M.L. Bolognesi, A. Cavalli, C. Melchiorre, V. Andrisano, *ChemBioChem.* 8 (2007), 2152–2161. (b) H. Naiki, K. Higuchi, K. Nakakuki, T. Takeda, Kinetic Analysis of Amyloid Fibril Polymerization in vitro. *Lab. Investig. J. Tech. Methods Pathol.* 65 (1991) 104–110.
[47] (a) E. Peña-Altamira, E. Polazzi, E. Moretto, M. Lauriola, B. Monti. *Eur J Neurosci.* 39 (2014) 176-85. (b) E. Uliassi, L.E. Peña-Altamira, A.V. Morales, F. Massenzio, S. Petralla, M. Rossi, M. Roberti, L. Martinez Gonzalez, A. Martinez, B. Monti, M.L. Bolognesi. *ACS Chem Neurosci.* 10 (2019) 279-294.
[48] Schrödinger LLC, New York, USA (2018).
[49] Maestro, Schrödinger LLC, New York, USA (2018).
[50] LigPrep, Schrödinger LLC, New York, USA (2018).
[51] H. M. Berman, J. Westbrook, Z. Feng, G. Gilliland, T. N. Bahat, H. Weissig, I. N. Shindyalov, P. E. Bourne, *The Protein Data Bank. Nucleic Acids Res.*, 28 (2000) 235-242.
[52] J. Cheung, M. J. Rudolph, F. Burshteyn, M. S. Cassidy, E. N. Gary, J. Love, M. C. Franklin, J. J. Height, *J. Med. Chem.*, 55 (2012) 10282-10286.
[53] U. Kosak, B. Brus, D. Knez, S. Zakelj, J. Trontelj, A. Pislar, R. Sink, M. Jukic, M. Zivin, A. Podkowa, F. Nachon, X. Brazzolotto, J. Stojan, J. Kos, N. Coquelle, K. Salat, J. P. Colletier, S. Gobec, *J. Med. Chem.*, 61 (2018) 119-139.
[54] Protein Preparation Wizard, Schrödinger LLC, New York, USA (2018).
[55] Glide, Schrödinger LLC, New York, USA (2018).
[56] J. Li, R. Abel, K. Zhu, Y. Cao, S. Zhao, R. A. Friesner, *Proteins*, 79 (2011) 2794-2812.
[57] Prime, Schrödinger LLC, New York, USA (2018).
[58] Desmond Molecular Dynamics System, D. E. Shaw Research, New York, USA (2018).

In the case of our manuscript entitled "*N*-1,2,3-Triazole-Isatin Derivatives for Cholinesterase and β-Amyloid Aggregation Inhibition: *A Comprehensive Bioassay Study* by Marques *at al.* we declare no conflicts of interest.

N-1,2,3-Triazole-Isatin Derivatives for Cholinesterase and β-Amyloid Aggregation Inhibition: *A Comprehensive Bioassay Study*

Carolina S. Marques,[a*] Óscar López,[b] Donatella Bagetta,[c,d] Elisabete P. Carreiro,[a] Sabrina Petralla[e], Manuela Bartolini[e], Matthias Hoffmann[f], Stefano Alcaro[c,d], Barbara Monti[e], Maria Laura Bolonesa[e], Michael Decker[f], José G. Fernández-Bolaños[b] and Anthony J. Burke,[a,g*]

[a]Centro de Química de Évora, University of Évora, Institute for Research and Advanced Studies, Rua Romão Ramalho, 59, 7000 Évora, Portugal
[b]Departamento de Química Orgánica, Facultad de Química, Universidad de Sevilla, Apartado 1203, E-41071, Seville, Spain
[c]Net4Science Academic Spin-Off, University "Magna Græcia" of Catanzaro, Campus Universitario "S.Venuta", Catanzaro, Italy
[d]Department of "Scienze della Salute", University "Magna Græcia" of Catanzaro, Campus Universitario "S.Venuta", Catanzaro, Italy
[e]Department of Pharmacy and Biotechnology, Alma Mater Studiorum, University of Bologna, via Belmeloro 6, 40126 Bologna, Italy.
[f] Pharmaceutical and Medicinal Chemistry, Institute of Pharmacy and Food Chemistry, Julius Maximilian University Würzburg, Am Hubland, D-97074 Würzburg, Germany.
[g]Chemistry Department, School of Science and Technology, University of Évora, Rua Romão Ramalho 59, 7000-671 Évora, Portugal.

Supporting Information

Contents

1. Re-docking figures of *h*ChEs co-crystallized ligands

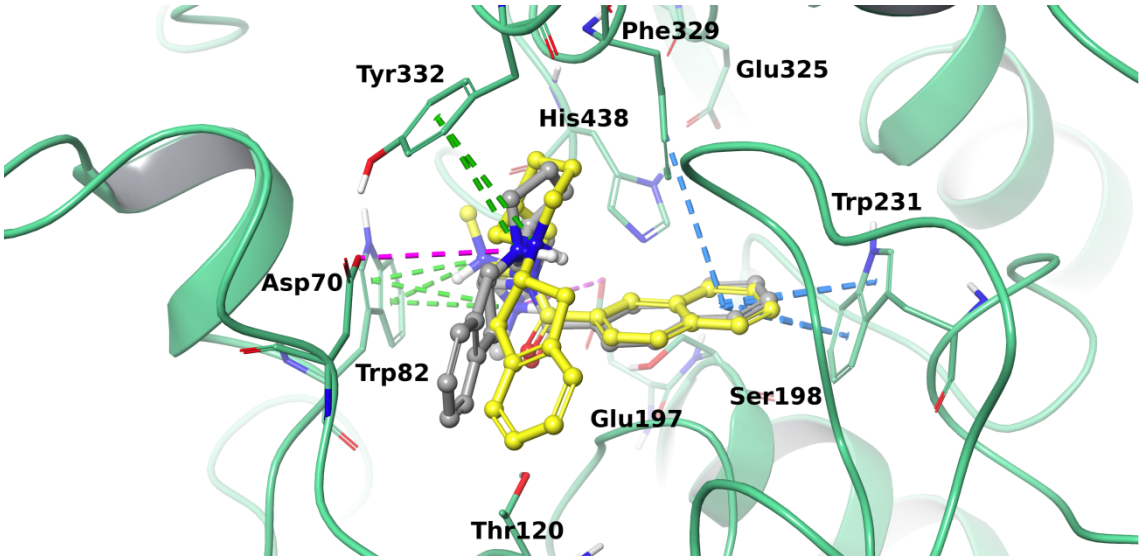

Figure s1. Superimposition of the re-docked (yellow carbons) and co-crystallized (grey carbons) N-((1-(2,3-dihydro-1H-inden-2-yl)piperidin-3-yl)methyl)-N-(2-(dimethylamino)ethyl)-2-naphtamide binding mode. RMSD was found to be 1.48 Å. The enzyme is represented in green cartoons, the most relevant interacting residues and the catalytic triad are depicted as thin tubes and the ligand is shown in ball and stick representation. π-π interactions, π-cation interactions and salt bridges are respectively represented in light-blue, green and pink.

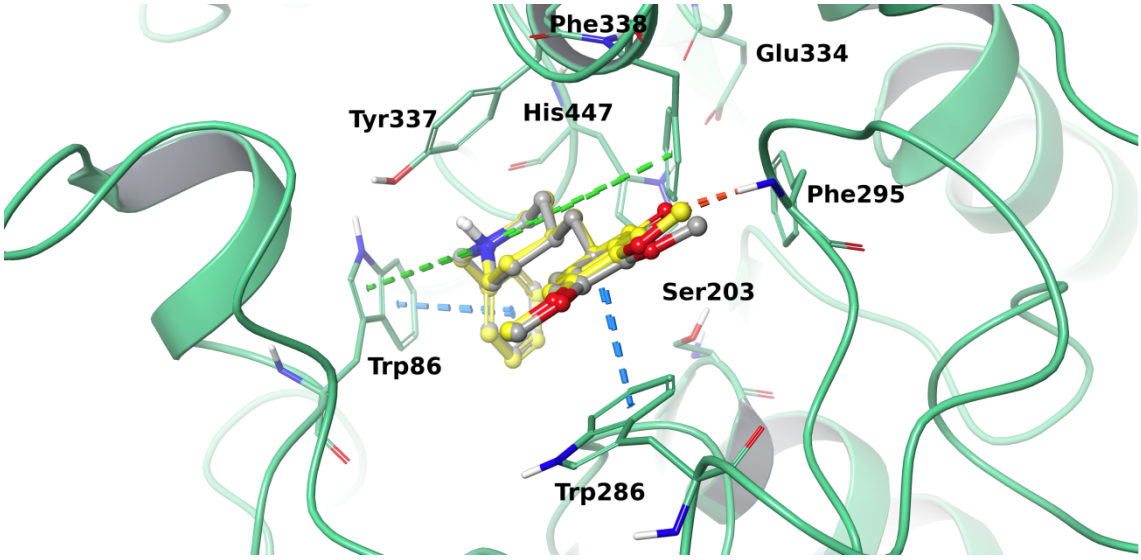

Figure s2. Superimposition of the re-docked (yellow carbons) and co-crystallized (grey carbons) Donepezil binding mode. RMSD was found to be 0.20 Å. The enzyme is represented in green cartoons, the most relevant interacting residues and the catalytic triad are depicted in thin tubes and the ligand is shown in ball and stick representation π-π interactions, π-cation interactions and hydrogen bonds are respectively represented in light-blue, green and orange.

2. ^{1}H and ^{13}C NMR spectra of the compounds (2j) and (2k)

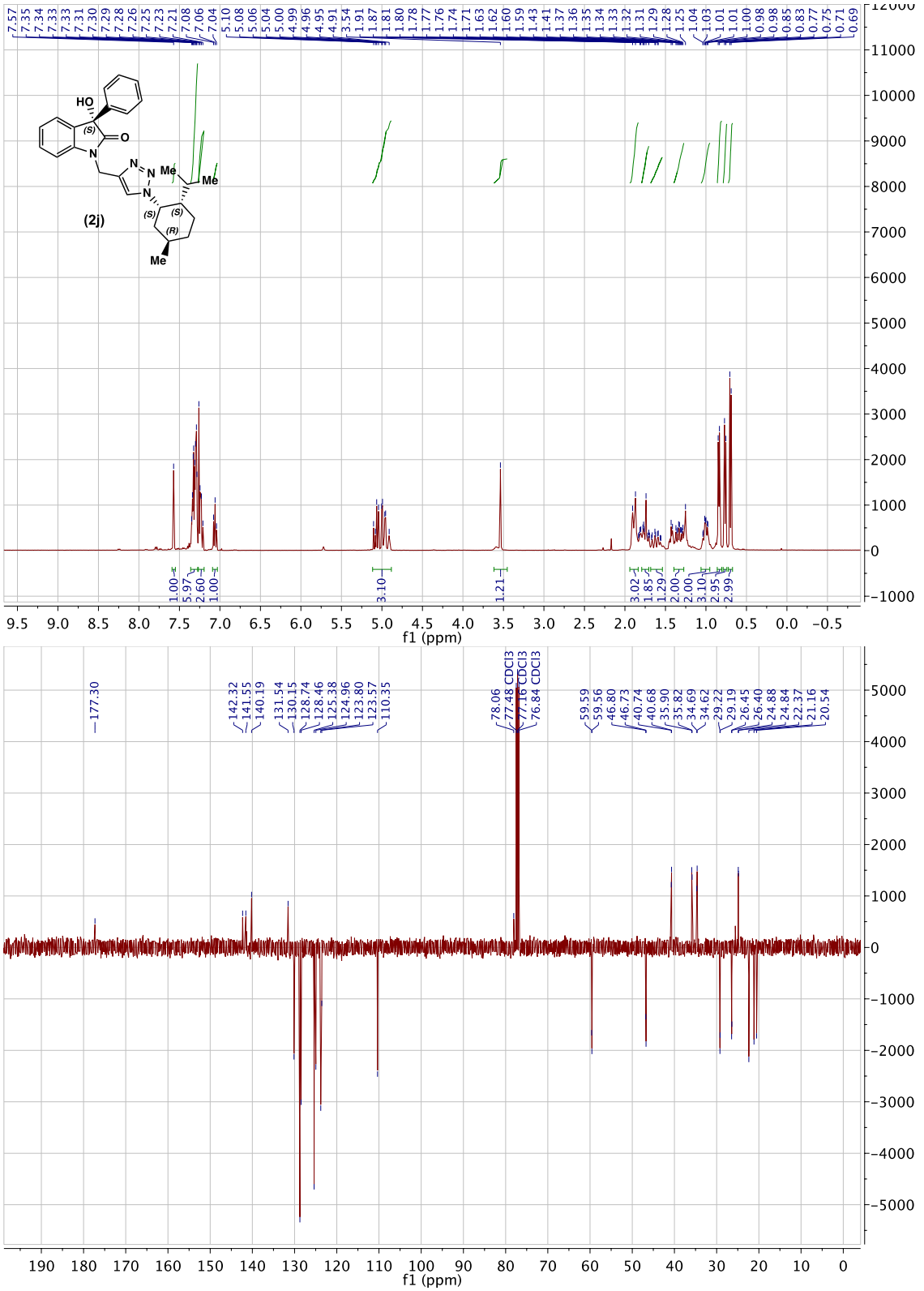

Figure s3. Compound **(2j)** in $CDCl_3$, (top) ^{1}H NMR and (bottom) ^{13}C NMR.

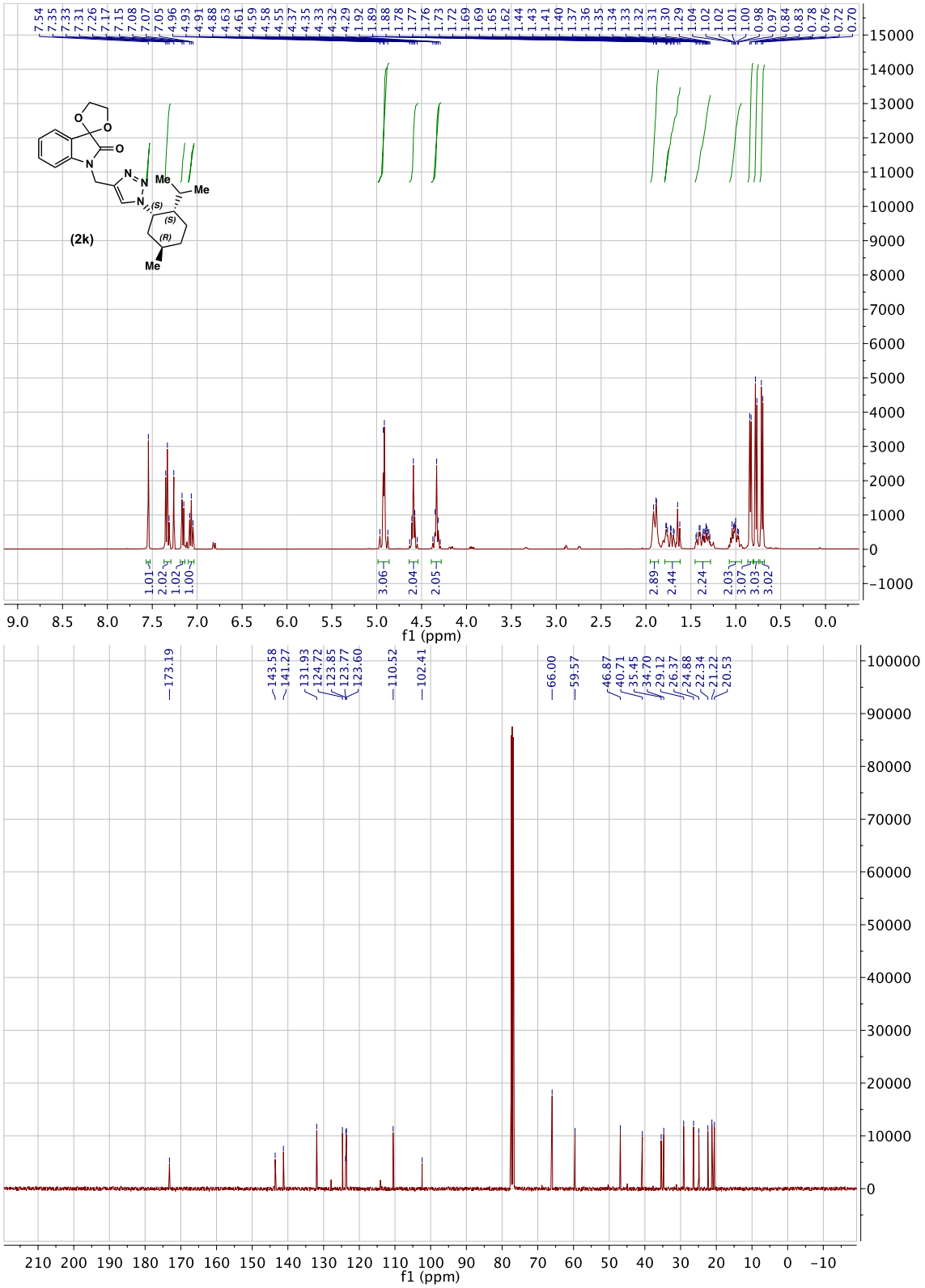

Figure s4. Compound **(2k)** in $CDCl_3$, (top) ^{1}H NMR and (bottom) ^{13}C NMR.

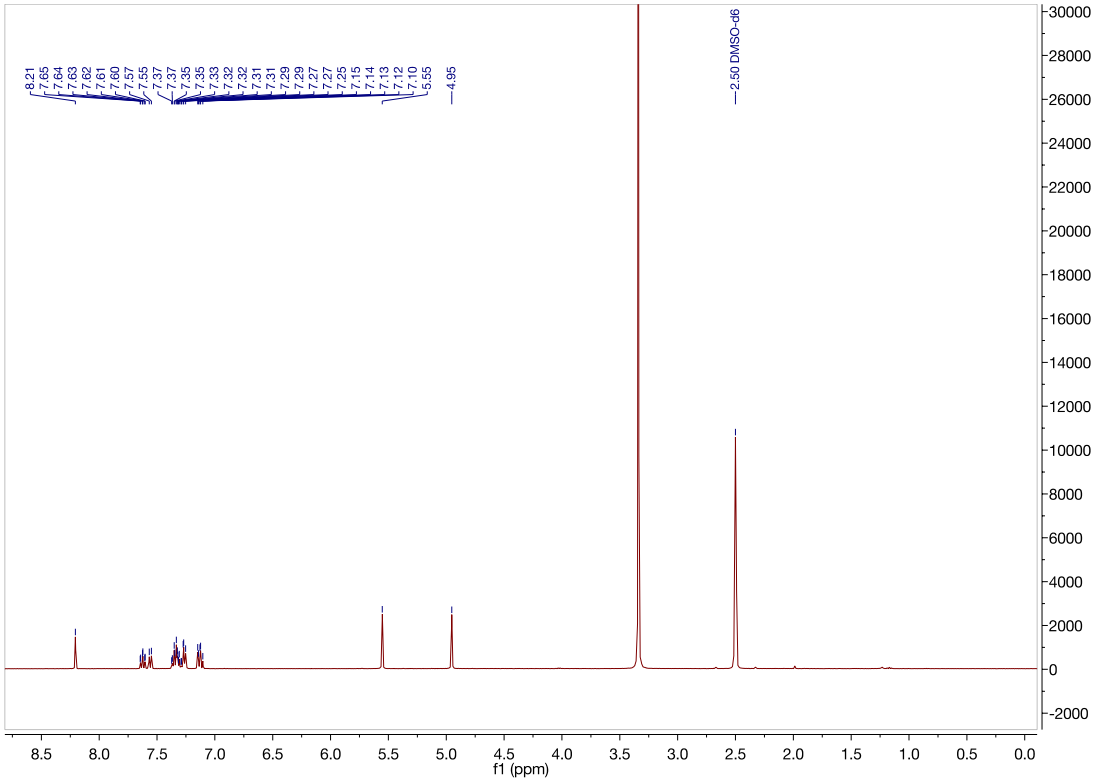

Figure s5. ^{1}H NMR spectrum of compound **(1a)** in DMSO-d_6, the reference spectrum for the STD-NMR studies.

(a)

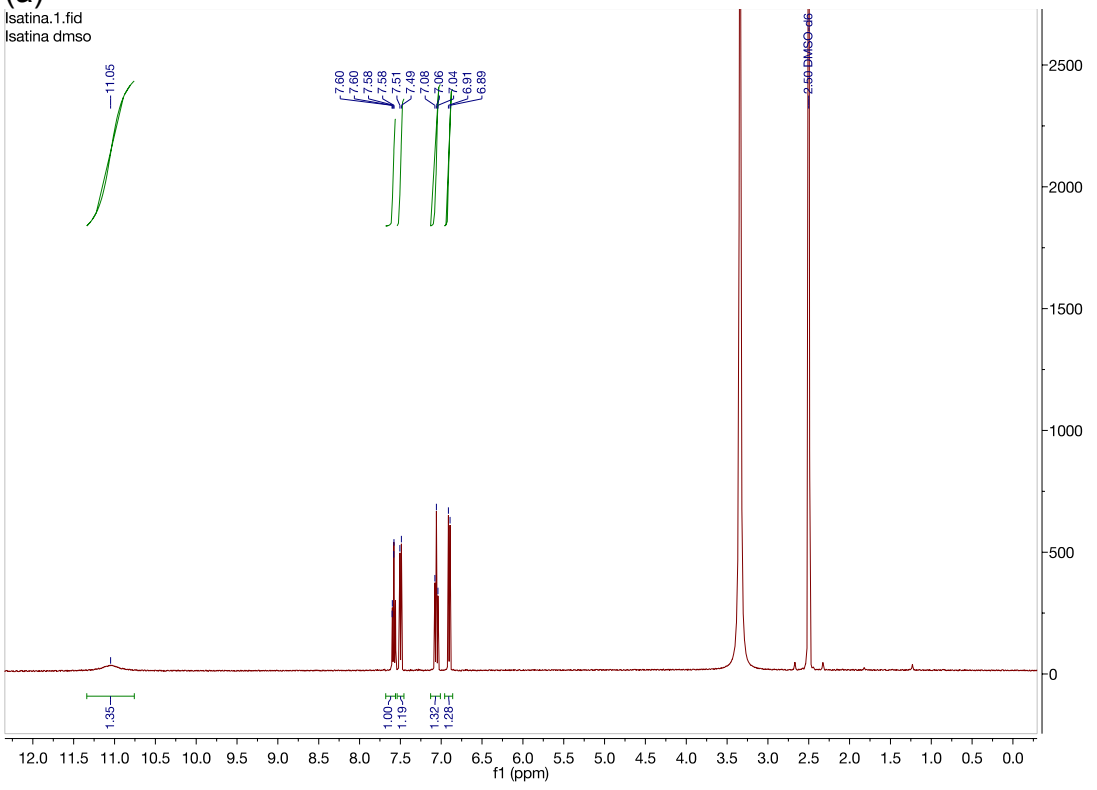

(b)

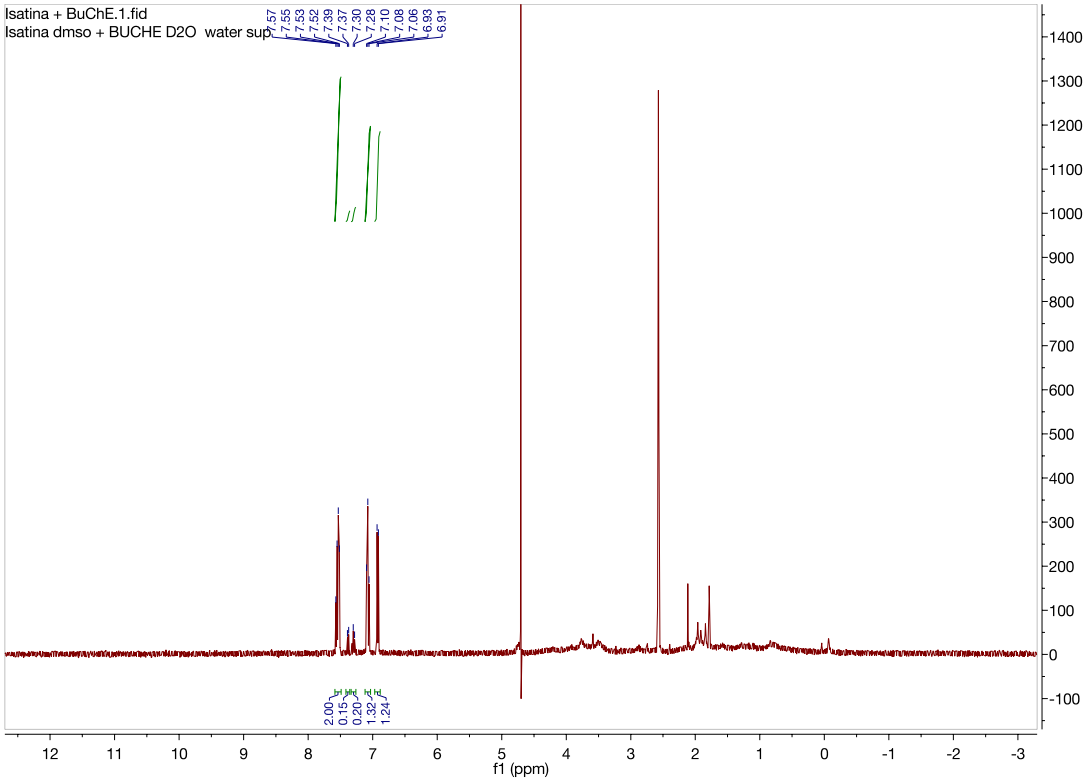

Figure s6. (a) ^{1}H NMR spectrum of isatin in DMSO-d_6. (b) ^{1}H NMR spectra of Isatin with *eq*BuChE. [Isatin]=0.8 mM in DMSO-d_6. [*eq*BuChE]= 4 µM in D_2O

(a)

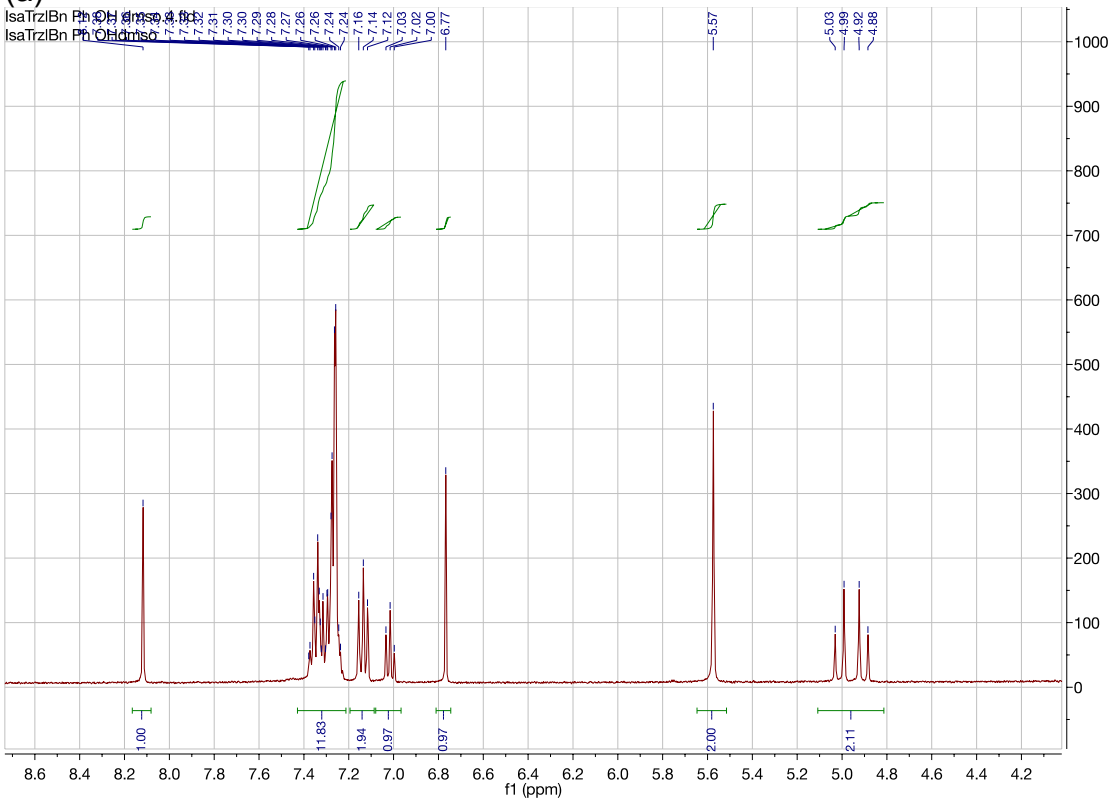

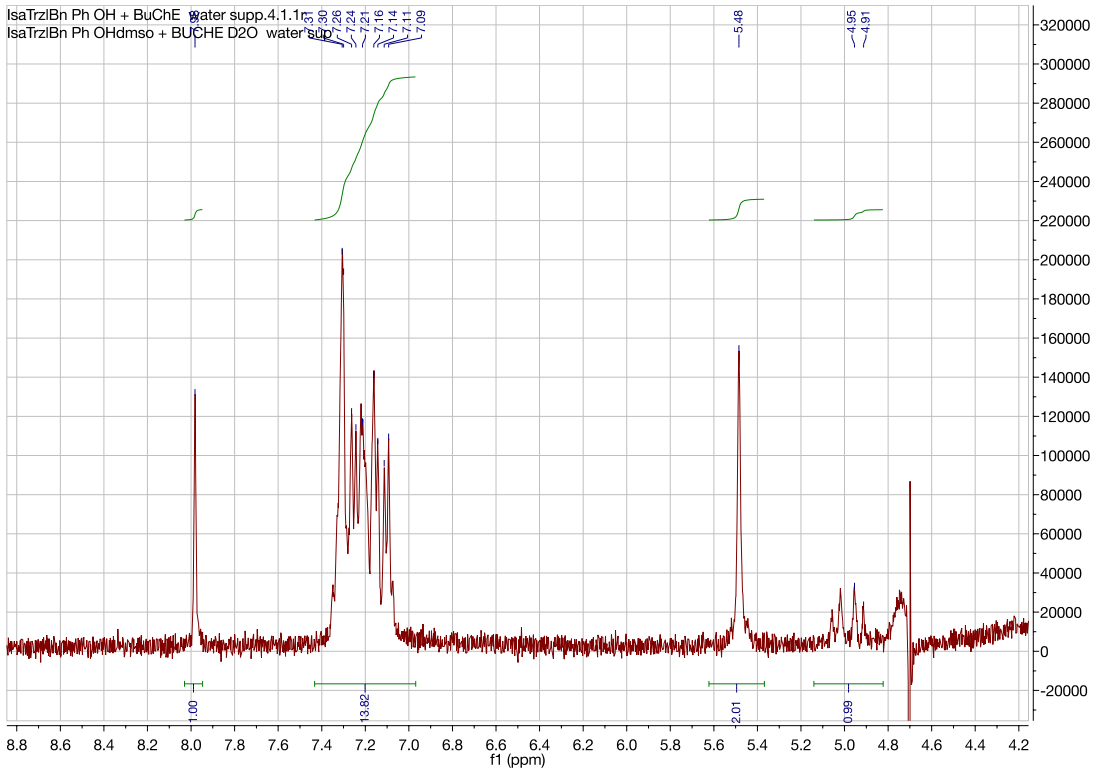

Figure s7. (a) ^{1}H NMR spectrum of compound **(2a)** in DMSO-d_6. (b) Truncated ^{1}H NMR spectra of **(2a)** with *eq*BuChE. (**(2a)** (0.8 mM) and *eq*BuChE (4µM)).

3. Cholinesterase Assays and Enzyme kinetics

Table s.1. Screening of the *N*-1,2,3-triazole-isatin derivatives **(1)** and **(2)** against *eq*BuChE, *ee*AChE and *h*BuChE Inhibition @100 µM.

Entry	Compound[a]	***ee*AChE Inhibition** (% inhibition ± SD)[b]	***eq*BuChE Inhibition** (% inhibition ± SD)[b]	***h*BuChE Inhibition** (% Inhibition ± SD)[b]
1	**1a**	31 ± 8	90 ± 0	97 ± 1.5
2	**1b**	42 ± 3	100 ± 0	99 ± 0.2
3	**1c**	46 ± 2	100 ± 0	85 ± 4.4
4	**2a**	31 ± 3	86 ± 1	91 ± 0.9
5	**2b**	Not soluble	Not soluble	Not soluble
6	**2c**	21 ± 5	94 ± 2	82 ± 1.3
7	**2d**	14 ± 4	72 ± 1	36 ± 3.9
8	**2e**	40 ± 4	77 ± 4	41 ± 6.2
9	**2f**	30 ± 3	66 ± 4	47 ± 1.5
10	**2g**	33 ± 3	54 ± 1	26 ± 1.9
11	**2h**	No inhibition	50 ± 4	21 ± 6.2

12	**2i**	17 ± 4	70 ± 2	46 ± 7.2
13	**2j**	34 ± 2	100 ± 0	94 ± 1.6
14	**2k**	73 ± 2	100 ± 0	23 ± 1.4
15	**Galantamine**	100[c]	100[d]	

[a]See structures in Schemes 1 and 2 main paper.
[b][I] = 100 μM; [S] = 29.0 μM for *ee*AChE, 18.4 μM for *eq*BuChE, 452 μM for *h*BChE. Data are expressed as mean ± standard deviation (SD) for two independent measurements
[c]K_{ia}= 1.0 ± 0.3 μM (competitive inhibition)
[d]K_{ia}= 6.2 ± 0.4 μM (competitive inhibition)

Cornish-Bowden plots[1]

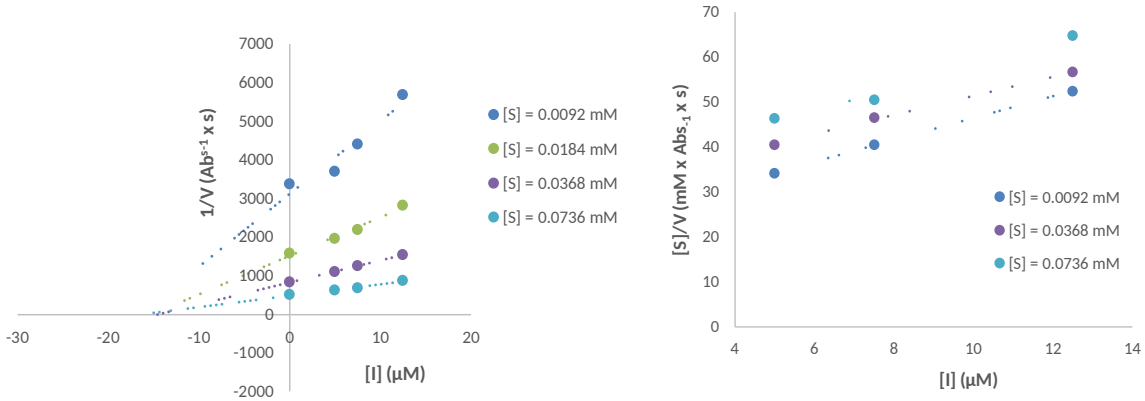

Figure s8. Compound (1a)

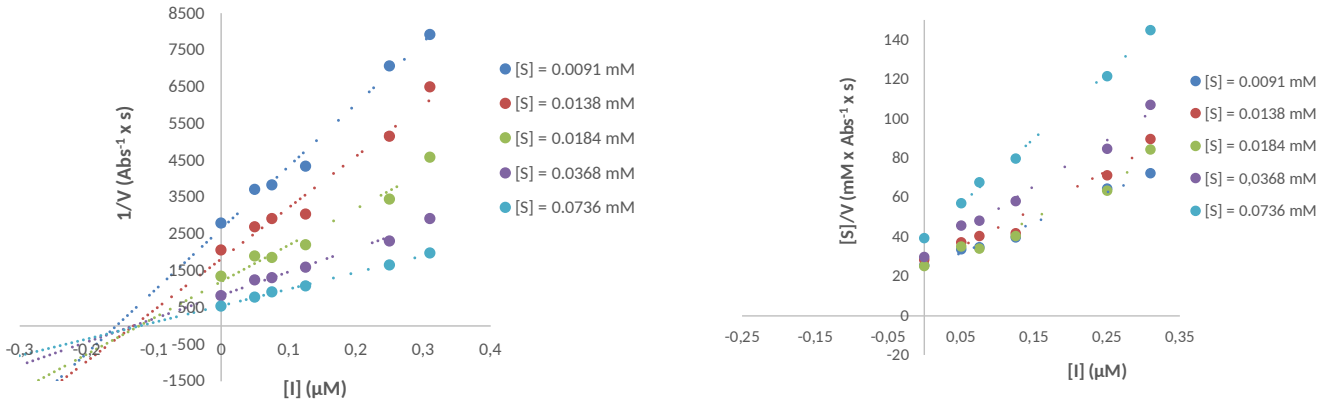

Figure s9. Compound (1b).

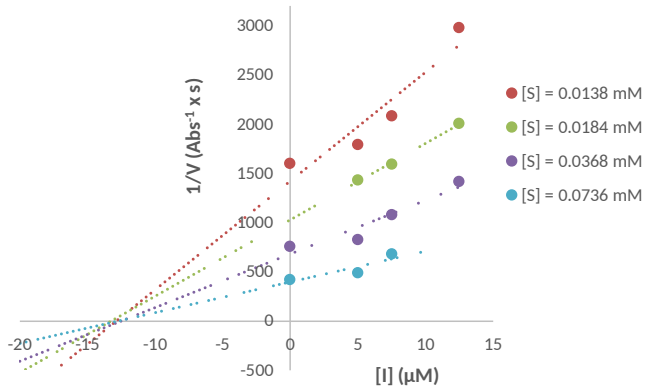

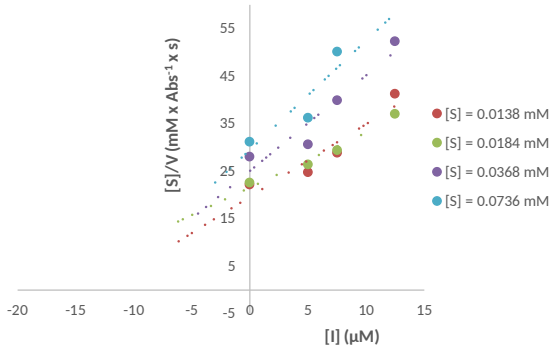

Figure s10. Compound (1c).

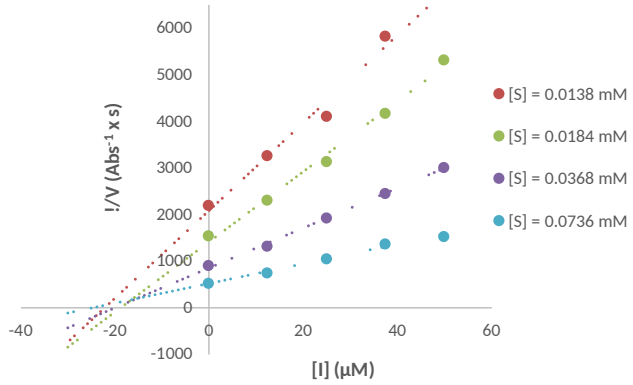

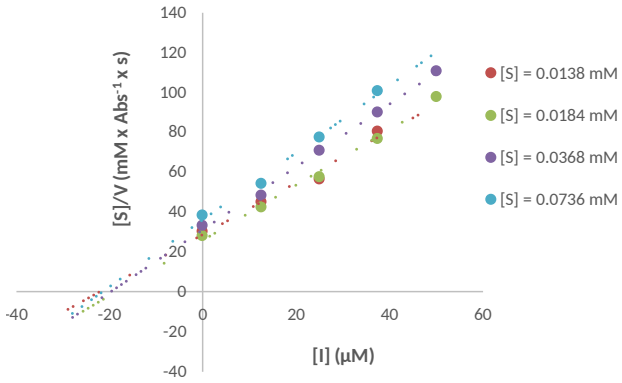

Figure s11. Compound (2a).

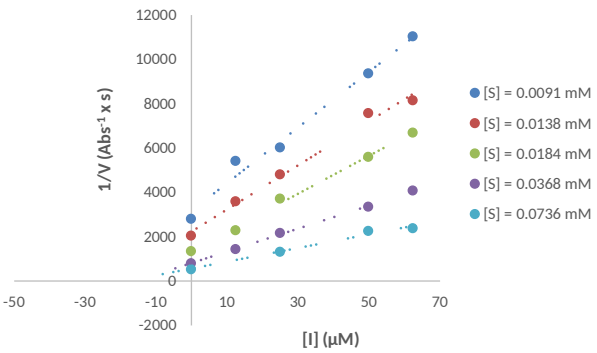

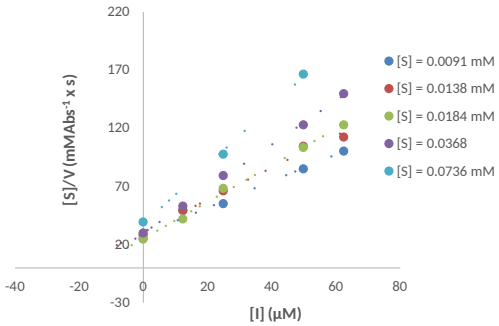

Figure s12. Compound (2c).

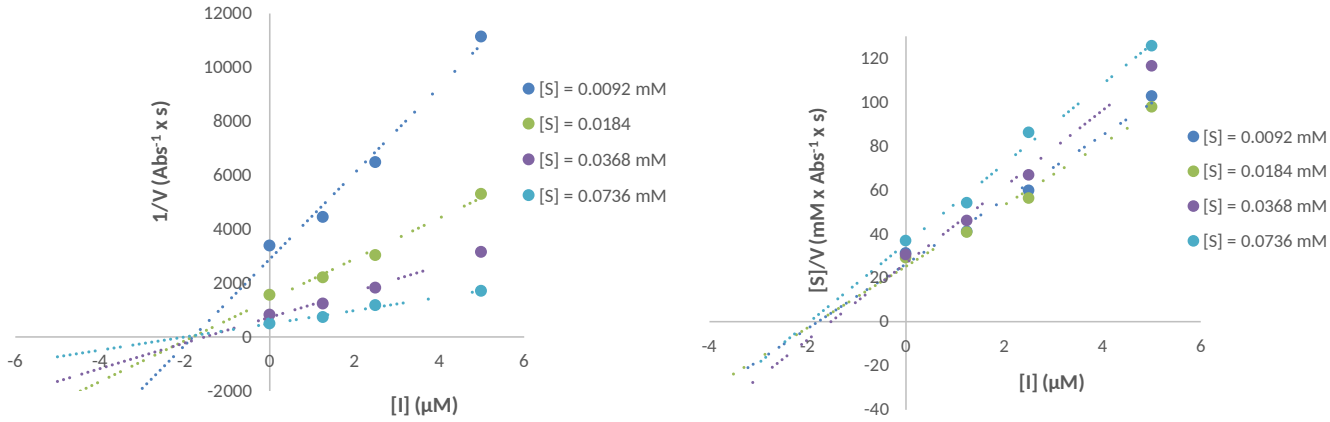

Figure s13. Compound (2j).

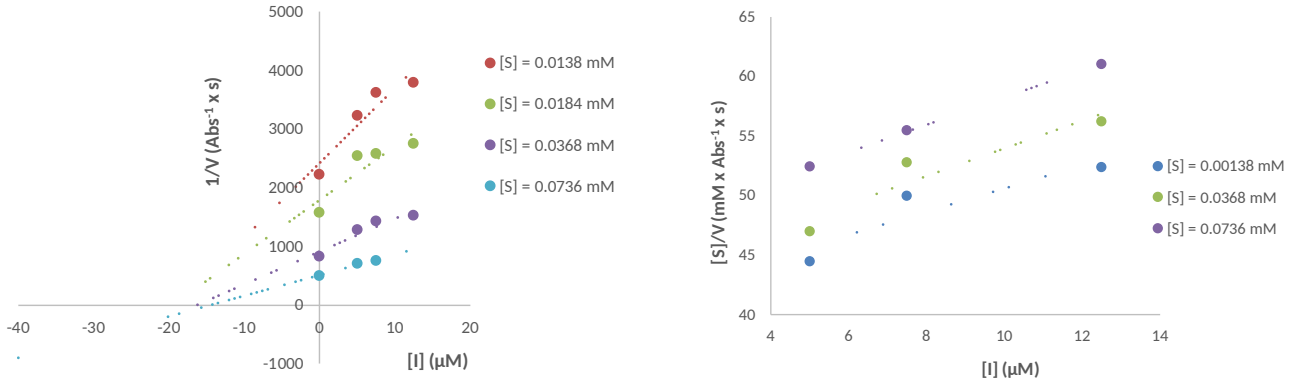

Figure s14. Compound (2k).

Galantamine

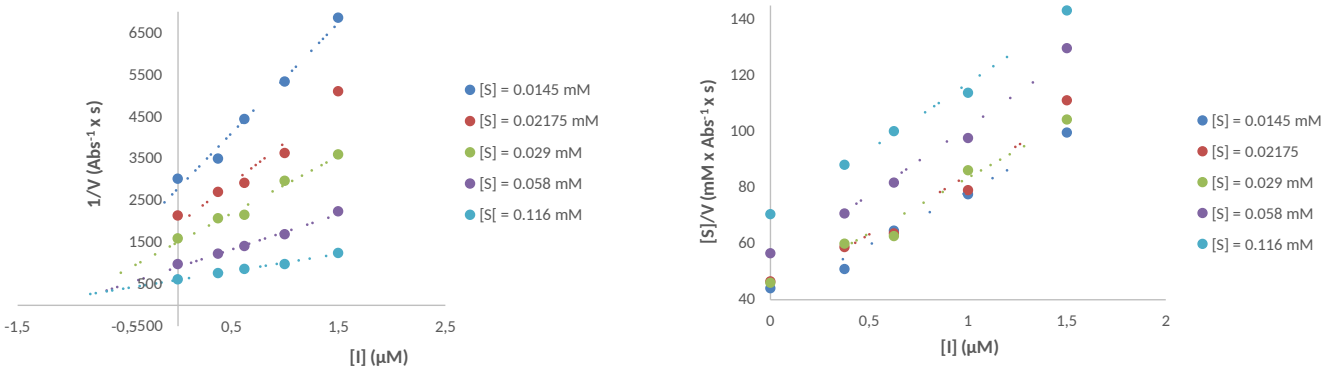

Figure s15. Inhibition of AChE with Galantamine.

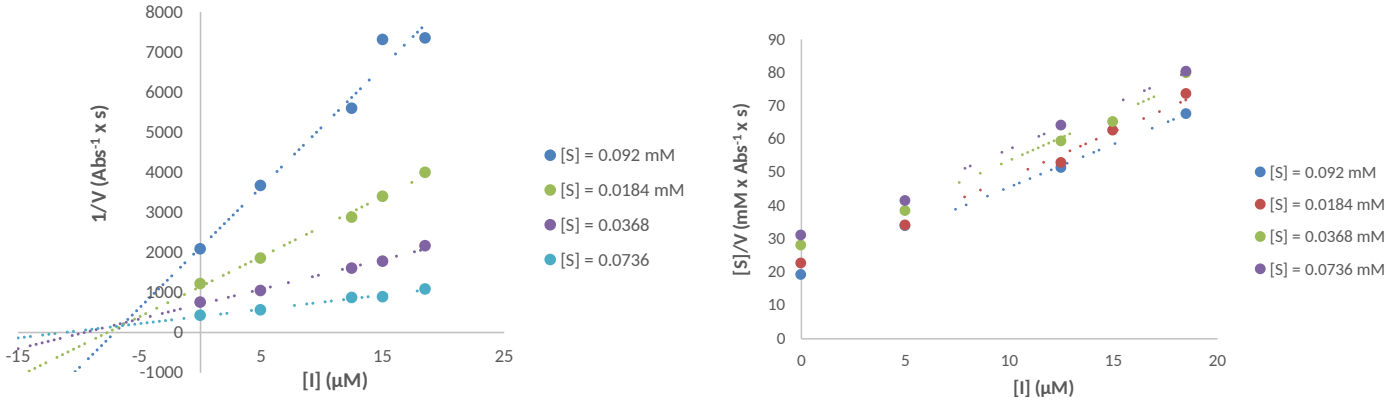

Figure s16. Inhibition of BuChE with Galantamine.

References

1. A. Cornish-Bowden, *Biochem. J.* 137 (1974) 143-144.